

Don't Overlook the Support Set: Towards Improving Generalization in Meta-learning

Huaxiu Yao*, Longkai Huang†, Ying Wei‡, Li Tian§, Junzhou Huang¶, Zhenhui Li||

Abstract

Meta-learning has proven to be a powerful paradigm for transferring the knowledge from previously tasks to facilitate the learning of a novel task. Current dominant algorithms train a well-generalized model initialization which is adapted to each task via the support set. The crux, obviously, lies in optimizing the generalization capability of the initialization, which is measured by the performance of the adapted model on the query set of each task. Unfortunately, this generalization measure, evidenced by empirical results, pushes the initialization to overfit the query but fail the support set, which significantly impairs the generalization and adaptation to novel tasks. To address this issue, we include the support set when evaluating the generalization to produce a new meta-training strategy, MetaMix, that linearly combines the input and hidden representations of samples from both the support and query sets. Theoretical studies on classification and regression tasks show how MetaMix can improve the generalization of meta-learning. More remarkably, MetaMix obtains state-of-the-art results by a large margin across many datasets and remains compatible with existing meta-learning algorithms.

1 Introduction

Meta-learning, or learning to learn [38], empowers agents with the core aspect of intelligence—quickly learning a new task with as little as a few examples by drawing upon the knowledge learned from prior tasks. The resurgence of meta-learning recently pushes ahead with more effective algorithms that have been deployed in areas such as computer vision [16, 22, 37], natural language processing [6, 13, 25], and robotics [44, 49]. Some of the dominant algorithms learn a transferable metric space from previous tasks [30, 35, 41], unfortunately being only applicable to classification problems. Instead, gradient-based algorithms [7, 9, 21] framing meta-learning as a bi-level optimization problem are flexible and general enough to be independent of problem types, which we focus on in this work.

The bi-level optimization procedure of gradient-based algorithms is illustrated in Figure 1. In the inner-loop, the initialization of a model globally shared across tasks (i.e., θ_0) is adapted to each task (e.g., ϕ_1 for the first task) via gradient descent over the support set of the task. To reach the desired goal that optimizing from this initialization leads to fast adaptation and generalization, a

*Pennsylvania State University; e-mail: huaxiuyao@psu.edu

†Nanyang Technological University; e-mail: lhuang018@e.ntu.edu.sg

‡Tencent AI Lab; e-mail: judyweiying@gmail.com

§Tencent AI Lab; e-mail: litiantian@tencent.com

¶Tencent AI Lab; e-mail: jzhuang@uta.edu

||Pennsylvania State University; e-mail: jessiel@psu.edu

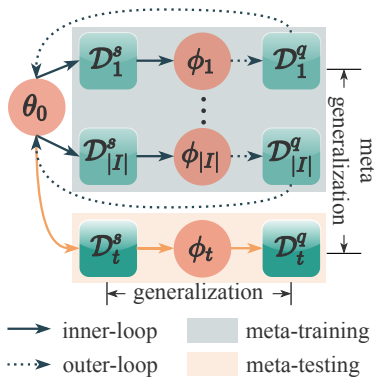


Figure 1: Illustrations of the meta-learning process and two types of generalization.

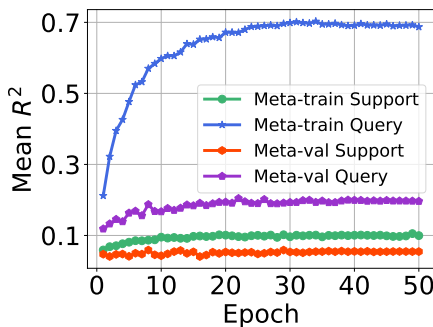


Figure 2: Inconsistent behaviors of the learned initialization on the support and query set.

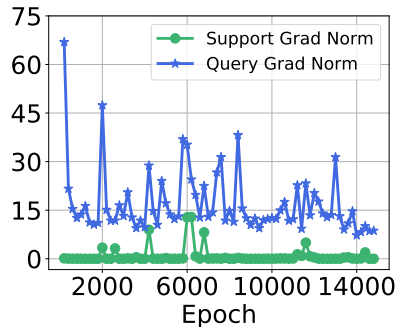


Figure 3: Gradient norms of support and query sets under the Omniglot 5-way 1-shot setting.

meta-training objective evaluating the generalization capability of the initialization on all meta-training tasks is optimized in the outer-loop. Specifically, the generalization capability on each task is measured by the performance of the adapted model on a set distinguished from the support, namely the query set.

The learned initialization, however, is at high risk of overfitting the meta-training tasks and failing a meta-testing task. As evidenced in Figure 2 for drug activity prediction which we detail later in experiments, the prediction accuracy of the learned initialization without adaptation is exceptionally high on query sets of meta-training tasks but surprisingly low on those of meta-testing ones. Improving this generalization from meta-training to meta-testing tasks, which we call meta-generalization, is especially challenging – standard regularizers like weight decay lose their power as they hurt the flexibility of fast adaptation in the inner-loop. To this end, the few existing solutions attempt to regularize the search space of the initialization [47] or enforce a fair performance of the initialization across all meta-training tasks [15] while preserving the expressive power for adaptation.

Rather than passively imposing regularizations on the initialization, we turn towards an active approach which anticipates more data to meta-train the initialization. The intuition comes from empirical implications from Figure 2. The huge gap between the prediction accuracy of the learned initialization on query sets and that on support sets suggests that the initialization overfits the query but overlooks the support set. This initialization, obviously, runs counter to a desired one which should be generalized enough to behave consistently across any set of meta-training tasks before being generalized to support sets of meta-testing tasks. To resolve the inconsistency and thereby promote meta-generalization, an intuitive solution is to evaluate and optimize the generalization capability of the initialization with more data than the query sets only in the outer-loop.

The most immediate choice for more data is the support sets, while it is far from enough. The support sets contribute little to the value and gradients of the meta-training objective, as the meta-training objective is formulated as the performance of the adapted model which is exactly optimized via support sets. Figure 3 sheds light on this fact, where the gradient norms of the meta-training objective with regard to the initialization by support sets are much smaller than those by query sets. Thus, in this paper, we are motivated to produce “more” data out of the accessible support and query sets. The resulting strategy we propose, **MetaMix**, linearly combines either original features or hidden representations of the support and query sets, and performs the same linear interpolation between their corresponding labels. These additional signals for the meta-training

objective encourage the learned initialization to be consistently generalized to a spectrum of data from the support to the query sets, thereby improving the meta-generalization as expected.

Not only do we identify this novel direction to improve meta-generalization, we also offer theoretical insights into the reason why MetaMix works in both classification and regression problems. More remarkably, throughout comprehensive experiments, we demonstrate three significant benefits of MetaMix. First, the performances are substantially improved over state-of-the-art meta-learning algorithms and the two regularizers [15, 47] in various real-world datasets. Second, better generalization to even heterogeneous tasks is achieved. Third, MetaMix is compatible with existing and advanced meta-learning algorithms and ready to give a boost to their performances.

2 Preliminaries

Gradient-based meta-learning algorithms assume a set of tasks to be sampled from a distribution $p(\mathcal{T})$. Each task \mathcal{T}_i consists of a support sample set $\mathcal{D}_i^s = \{(\mathbf{x}_{i,j}^s, \mathbf{y}_{i,j}^s)\}_{j=1}^{K^s}$ and a query sample set $\mathcal{D}_i^q = \{(\mathbf{x}_{i,j}^q, \mathbf{y}_{i,j}^q)\}_{j=1}^{K^q}$, where K^s and K^q denote the number of source and query samples, respectively. The objective of meta-learning is to master new tasks quickly by adapting a well-generalized model learned over the task distribution $p(\mathcal{T})$. Specifically, the model f parameterized by θ is trained on massive tasks sampled from $p(\mathcal{T})$ during meta-training. When it comes to meta-testing, f is adapted to a new task \mathcal{T}_t with the help of the support set \mathcal{D}_i^s and evaluated on the query set \mathcal{D}_t^q .

Take model-agnostic meta-learning (MAML) [7] as an example. The well-generalized model is grounded to an initialization for f , i.e., θ_0 , which is adapted to each i -th task in a few gradient steps by its support set \mathcal{D}_i^s . The generalization performance of the adapted model, i.e., ϕ_i , is measured on the query set \mathcal{D}_i^q , and in turn used to optimize the initialization θ_0 during meta-training. Let \mathcal{L} and μ denote the loss function and the inner-loop learning rate, respectively. The above interleaved process is formulated as a bi-level optimization problem,

$$\theta_0^* := \min_{\theta_0} \mathbb{E}_{\mathcal{T}_i \sim p(\mathcal{T})} [\mathcal{L}(f_{\phi_i}(\mathbf{X}_i^q), \mathbf{Y}_i^q)], \text{ s.t. } \phi_i = \theta_0 - \mu \nabla_{\theta} \mathcal{L}(f_{\theta}(\mathbf{X}_i^s), \mathbf{Y}_i^s), \quad (1)$$

where $\mathbf{X}_i^{s(q)}$ and $\mathbf{Y}_i^{s(q)}$ represent the concatenation of samples and their corresponding labels for the support (query) set, respectively. In the meta-testing phase, to solve the new task \mathcal{T}_t , the optimal initialization θ_0^* is fine-tuned on its support set \mathcal{D}_i^s to the resulting task-specific parameters ϕ_t .

3 MetaMix

In practical situations, the distribution $p(\mathcal{T})$ is unknown for estimation of the expected performance in Eqn. (14). Instead, the common practice is to approximate it with the empirical performance, i.e.,

$$\theta_0^* := \min_{\theta_0} \frac{1}{n_T} \sum_{i=1}^{n_T} [\mathcal{L}(f_{\phi_i}(\mathbf{X}_i^q), \mathbf{Y}_i^q)], \text{ s.t. } \phi_i = \theta_0 - \mu \nabla_{\theta} \mathcal{L}(f_{\theta}(\mathbf{X}_i^s), \mathbf{Y}_i^s). \quad (2)$$

Unfortunately, this empirical risk observes the generalization ability of the initialization θ_0 only at a finite set of n_T tasks. When the function f is sufficiently powerful, a trivial solution of θ_0 is to memorize all tasks [47]. Such memorization leads to poor meta-generalization (see Figure 1) of θ_0 to meta-testing tasks. Before proceeding to our solution for improving the meta-generalization, we would first consider what has been memorized. Since θ_0 is optimized for its generalization performance on all query sets in the outer-loop, the query sets $\{\mathcal{D}_i^q\}_{i=1}^{n_T}$ are memorized specifically.

Inspired by data augmentation [5, 50, 51] which is used to mitigate the memorization of training samples in conventional supervised learning, we propose to alleviate the problem of task memorization via involving more data to meta-train θ_0 . Compared to supervised learning where the augmentation originates from only the memorized training samples, better yet, we also have access to the support sets $\{\mathcal{D}_i^s\}_{i=1}^{n_T}$ besides the memorized query sets during meta-training. Besides, Figure 2 shows that θ_0 , as a sign of poor meta-generalization, behaves very differently on the query and the support sets.

Therefore, we are highly motivated to propose MetaMix that produces more data to meta-train θ_0 by mixing samples from both query sets and support sets. The strategy of mixing follows Manifold Mixup [40] where not only inputs but also hidden representations are mixed up. Assume that the model f consists of L layers. The hidden representation of a sample set \mathbf{X} at the l -th layer is denoted as $f_{\theta^l}(\mathbf{X})$ ($0 \leq l \leq L-1$), where $f_{\theta^0}(\mathbf{X}) = \mathbf{X}$. For a pair of support and query sets with their corresponding labels in the i -th task \mathcal{T}_i , i.e., $(\mathbf{X}_i^s, \mathbf{Y}_i^s)$ and $(\mathbf{X}_i^q, \mathbf{Y}_i^q)$, we randomly sample a value of $l \in \mathcal{C} = \{0, 1, \dots, L-1\}$ and compute the mixed batch of data for meta-training as,

$$\mathbf{X}_{i,l}^{mix} = \lambda f_{\phi^l}(\mathbf{X}_i^s) + (\mathbf{I} - \lambda) f_{\phi^l}(\mathbf{X}_i^q), \quad \mathbf{Y}_i^{mix} = \lambda \mathbf{Y}_i^s + (\mathbf{I} - \lambda) \mathbf{Y}_i^q, \quad (3)$$

where $\lambda = \text{diag}(\{\lambda_j\}_{j=1}^{K^s})$ and each coefficient $\lambda_j \sim \text{Beta}(\alpha, \beta)$. Here, we assume that the size of the support set and that of the query are equal, i.e., $K^s = K^q$. If $K^s < K^q$, for each data sample in the query set, we randomly select one sample from support set for mixup. In Appendix B.1, we illustrate the Beta distribution in both symmetric (i.e., $\alpha = \beta$) and skewed shapes (i.e., $\alpha \neq \beta$). Using the mixed batch by MetaMix, we reformulate the outer-loop optimization problem as,

$$\theta_0^* := \min_{\theta_0} \frac{1}{n_T} \sum_{i=1}^{n_T} \mathbb{E}_{\lambda \sim \text{Beta}(\alpha, \beta)} \mathbb{E}_{l \sim \mathcal{C}} [\mathcal{L}(f_{\phi^{L-l}}(\mathbf{X}_{i,l}^{mix}), \mathbf{Y}_i^{mix})], \quad (4)$$

where $f_{\phi^{L-l}}$ represents the rest of layers after the mixed layer l . MetaMix is flexible enough to be compatible with off-the-shelf gradient-based meta-learning algorithms, by replacing the query sets with the mixed batch for meta-training. Taking MAML with MetaMix as an example, we show meta-training and meta-testing in Alg. 1 and Alg. 2 of Appendix.

We also probe into the mechanism of MetaMix in improving the meta-regularization, by linking to generalization in the information theory [34]. In [34], the SGD optimization is suggested to have two phases, i.e., empirical error minimization and representation compression. The compression phase, taking much longer time, is accountable to generalization. Unfortunately, a few adaptation steps in the inner-loop only suffice to minimize the empirical error with regard to the support set but leave the hidden representations uncompressed. Thus, the adapted model tends to fail the query sets, so that the burden of minimizing the generalization performance in the outer-loop is placed onto θ_0 which gradually overfits to the query sets. MetaMix, by incorporating the support sets for the outer-loop optimization which requires sufficient iterations, pulls θ_0 back to behave consistently between the support and the query set and further compresses the hidden representations of the support set. Specifically, we computed the largest singular value for the hidden representations of the support set after meta-training. As Table 1 shows, MAML with MetaMix achieves a reduction of the top singular values, which signifies more compressed representations and thereby better generalization to the support set [28]. θ_0 with this consistent generalization across support and query is highly anticipated to generalize to meta-testing tasks.

4 Theoretic Analysis

In this section, we theoretically study the effectiveness of MetaMix in two special scenarios in classification and regression tasks. To show a general case, we omit the task-level index i for all associated symbols. The gradient and Hessian of the loss function \mathcal{L} computed on support set and query set are denoted by \mathbf{g}^s , \mathbf{H}^s , \mathbf{g}^q , \mathbf{H}^q , respectively. For brevity, we denote the gradients $\mathbf{g}^s(\theta_0)$, $\mathbf{g}^q(\theta_0)$, $\mathbf{g}^s(\phi)$ and $\mathbf{g}^q(\phi)$ by $\mathbf{g}_{\theta_0}^s$, $\mathbf{g}_{\theta_0}^q$, \mathbf{g}_{ϕ}^s and \mathbf{g}_{ϕ}^q . And similar simplification of notation is also applied on the Hessian computed by θ_0 and ϕ .

We first focus on the objective Eqn. (14) without MetaMix. As the task-specific model is updated by one-step GD as: $\phi = \theta_0 - \mu \mathbf{g}_{\theta_0}^s$, the gradient of Eqn. (14) w.r.t. θ_0 in the outer loop optimization is:

$$\nabla_{\theta_0} \mathcal{L}(f_{\phi}(\mathbf{X}^q), \mathbf{Y}^q) = (\mathbf{I} - \mu \mathbf{H}_{\theta_0}^s) \mathbf{g}_{\phi}^q. \quad (5)$$

Following the analysis in [29], we present the following lemma to study the approximation of $\nabla_{\theta_0} \mathcal{L}(f_{\phi}(\mathbf{X}^q), \mathbf{Y}^q)$ with first and second-order Taylor expansion of \mathbf{g}_{ϕ}^q around θ_0 .

Lemma 1 *The gradient of Eqn. (14) can be approximated by*

$$\nabla_{\theta_0} \mathcal{L}(f_{\phi}(\mathbf{X}^q), \mathbf{Y}^q) = (\mathbf{I} - \mu \mathbf{H}_{\theta_0}^s) \mathbf{g}_{\phi}^q = \mathbf{g}_{\theta_0}^q - \mu \nabla_{\theta} \langle \mathbf{g}_{\theta_0}^s, \mathbf{g}_{\theta_0}^q \rangle + \mathcal{O}(\mu^2). \quad (6)$$

Here $\langle \cdot, \cdot \rangle$ represents the inner product. The detailed proof for Lemma 1 is available in Appendix A.1.

Ignoring the term $\mathcal{O}(\mu^2)$, the approximated gradient in Eqn. (6), $\nabla_{\theta_0} \mathcal{L}(f_{\phi}(\mathbf{X}^q), \mathbf{Y}^q)$, can be consider as the gradient on θ_0 of a loss function defined as

$$\tilde{\mathcal{L}}(f_{\theta_0}) = \mathcal{L}(f_{\theta_0}(\mathbf{X}^q), \mathbf{Y}^q) - \mu \langle \mathbf{g}_{\theta_0}^s, \mathbf{g}_{\theta_0}^q \rangle. \quad (7)$$

Notice that θ_0 is updated by gradient-based optimizer with the gradient $\nabla_{\theta_0} \mathcal{L}(f_{\phi}(\mathbf{X}^q), \mathbf{Y}^q)$. When the gradient is approximated by Eqn. (6), the update of θ_0 is to approximately minimize the loss function (7). There are two terms in Eqn. (7). The first term is the loss $\mathcal{L}(f_{\theta_0})$ on the query set \mathcal{D}^q . The second term can be viewed as a regularizer to encourage the similarity between the gradients of $\mathcal{L}(f_{\theta_0})$ computed on the support and query sets. In this way, the inner loop optimization process driven by the support set can approximate the outer loop gradient descent on the query set. Thus, the task-specific model after fast adaptation is expected to have satisfactory generalization performance on query set. However, the learning rate μ in the inner loop is often a small value, resulting in the limited effect of the second term and finally pushing the model initialization to overfit the query set.

In MetaMix, instead, we introduce the support set into the outer-loop optimization by linearly combining it with the query set, i.e., $\mathbf{X}^{mix} = \lambda \mathbf{X}^s + (\mathbf{I} - \lambda) \mathbf{X}^q$, $\mathbf{Y}^{mix} = \lambda \mathbf{Y}^s + (\mathbf{I} - \lambda) \mathbf{Y}^q$. Denoting $\mathcal{D}^{mix} = \{\mathbf{X}^{mix}, \mathbf{Y}^{mix}\}$ and its gradient as $\mathbf{g}_{\theta_0}^{mix}$, the approximated loss function in Eqn. (7) turns to,

$$\tilde{\mathcal{L}}(f_{\theta_0}) = \mathcal{L}(f_{\theta_0}(\mathbf{X}^{mix}), \mathbf{Y}^{mix}) - \mu \langle \mathbf{g}_{\theta_0}^s, \mathbf{g}_{\theta_0}^{mix} \rangle. \quad (8)$$

Since the second term in Eqn. (8) is a regularizer to encourage the gradient computed by support sets to be similar to that of the first term, it is sufficient to focus on analyzing the first term. Here we study the effectiveness on both regression and classification scenarios. For brevity, we remove the subscript θ_0 and denote the loss $\mathcal{L}(f_{\theta_0}(\mathbf{x}_j^s), \mathbf{y}_j^s)$ and $\mathcal{L}(f_{\theta_0}(\mathbf{x}_j^q), \mathbf{y}_j^q)$ of sample j by \mathcal{L}_j^s and \mathcal{L}_j^q , respectively.

Table 1: Largest singular value for class C1-C5 on MiniImagenet 5-shot (details are discussed in Appendix B.3.).

Class	C1	C2	C3	C4	C5
MAML	29.81	29.03	29.74	29.08	28.83
MR-MAML	23.42	21.83	22.72	22.33	22.30
MetaMix	19.43	18.84	19.52	19.79	18.69

MetaMix for classification problem with double linear loss In classification problem, we consider a double linear loss $\mathcal{L}(f_\theta) = -\sum_j \mathbf{y}_j \ell^\top(f_\theta(\mathbf{x}_j))$ which is linear on both \mathbf{x}_j and \mathbf{y}_j . Assuming $\mathbf{z}_j = \ell^\top(f_\theta(\mathbf{x}_j))$, we expand the loss function on \mathcal{D}^{mix} as:

$$\mathcal{L}(f_{\theta_0}; \mathcal{D}^{mix}) = -\sum_j \mathbf{y}_j^{mix} \ell^\top(f_{\theta_0}(\mathbf{x}_j^{mix})) = \sum_j \lambda_j^2 \mathcal{L}_j^s + (1 - \lambda_j)^2 \mathcal{L}_j^q - \lambda_j(1 - \lambda_j)(\mathbf{y}_j^s \mathbf{z}_j^q{}^\top + \mathbf{y}_j^q \mathbf{z}_j^s{}^\top). \quad (9)$$

The full proof is available in Appendix A.2. In Eqn. (9), the first two terms are the original loss on support and query sets. By optimizing Eqn. (9), the original loss on both sets is minimized. Notice the objective can also be realized by simply combining the support and query sets in outer loop optimization. Compared to the simple combination of support and query sets in outer loop optimization, the improvements of MetaMix are mainly benefited from the third term, which can be interpreted to a cross set distillation loss and is known to improve generalization performance [14, 23].

MetaMix for least-squared regression problem In regression problem, we consider a least-squared loss $\mathcal{L}(f_\theta) = \sum_j \|\mathbf{y}_j - \theta^\top \mathbf{x}_j\|^2$ and assume the support set \mathbf{X}^s and the query set \mathbf{X}^q are both i.i.d. sampled from the same unknown distribution \mathcal{P}_r and the mapping function of distribution \mathcal{P}_r is defined as $\mathbf{y} = \mathbf{w}^\top \mathbf{x}$. As \mathbf{X}^s and \mathbf{X}^q are the same by expectation, we denote both of them by \mathbf{X} . And we assume the difference between support and query sets lies in the outputs \mathbf{Y}^s and \mathbf{Y}^q as the mapping function to generate \mathbf{Y}^s and \mathbf{Y}^q are polluted by noise. To be specific, we assume

$$\mathbf{Y}^s = (\mathbf{w} + \boldsymbol{\epsilon}^s)^\top \mathbf{X}, \quad \mathbf{Y}^q = (\mathbf{w} + \boldsymbol{\epsilon}^q)^\top \mathbf{X}, \quad (10)$$

where $\boldsymbol{\epsilon}^s$ and $\boldsymbol{\epsilon}^q$ are noises sampled from a zero-mean distribution. To verify the existence of Eqn. (10), we illustrate a simple case that satisfy the equation in Appendix A.3. Caused by the existing noises, training the meta-model with either support set or query set are not able to recover the genuine model \mathbf{w} . But if we optimize on the MetaMix loss function, we can recover the genuine model as:

$$\begin{aligned} \mathcal{L}(f_{\theta_0}(\mathbf{X}^{mix}), \mathbf{Y}^{mix}) &= \|\mathbb{E}_{\lambda \sim \text{Beta}(\alpha, \alpha)}[\lambda \mathbf{Y}^s + (1 - \lambda) \mathbf{Y}^q] - \theta^\top \mathbf{X}\|^2 \\ &= \left\| \left(\mathbf{w} + \mathbb{E} \left[\frac{\boldsymbol{\epsilon}^s + \boldsymbol{\epsilon}^q}{2} \right] \right)^\top \mathbf{X} - \theta^\top \mathbf{X} \right\|^2 = \|(\mathbf{w} - \theta)^\top \mathbf{X}\|^2. \end{aligned} \quad (11)$$

The deduction of the second equality is available in Appendix A.3. The result in Eqn. (11) indicates that to minimize the loss function estimated on the data set with MetaMix is the same as to minimize the loss function estimated on clear data. Therefore, MetaMix strategy could recover the unbiased model, which improves the meta-generalization performance in regression problem.

5 Discussion with Related Works

One influential line of meta-learning algorithms is learning a transferable metric space between samples from previous tasks [27, 30, 35, 41, 48], which classify samples via lazy learning with the learned distance metric (e.g., Euclidean distance [35], cosine distance [41]). However, their applications are limited to classification problems, being infeasible in other problems (e.g., regression). In this work, we focus on gradient-based meta-learning algorithms learn a well-generalized model initialization from meta-training tasks [8, 7, 9, 10, 12, 20, 21, 31, 33], being agnostic to problems. This initialization is adapted to each task via the support set, and in turn the initialization is updated by maximizing the generalization performance on the query set. These approaches are at high risk of overfitting the meta-training tasks and generalizing poorly to meta-testing tasks.

Common techniques increase the generalization capability via regularizations such as weight decay [17], dropout [11, 36], and incorporating noise [2, 3, 39]. As mentioned in the ending paragraph of Section 3, the adapted model by only a few steps in the support set in the inner-loop likely performs poorly on the query set. To improve such generalization for better adaptation, either the number of parameters to adapt is reduced [32, 52] or adaptive noise is added [19]. The contribution of addressing this inner-loop overfitting towards meta-regularization, though positive, is limited. Until very recently, two regularizers were proposed to specifically improve meta-generalization, including MR-MAML [47] which regularizes the search space of the initialization while meanwhile allows it to be sufficiently adapted in the inner-loop, and TAML [15] enforcing the initialization to behave similarly across tasks. Instead of imposing regularizers on the initialization, our work takes a completely novel direction by actively soliciting more data to meta-train the initialization. Note that MetaMix is more than just a simple application of conventional data augmentation strategies [5, 40, 50], which has been proved in both [19] and our experiments to have a very limited role. We initiate to involve more data in the outer-loop and to identify the indispensable role of support sets.

6 Experiments

To show the effectiveness of MetaMix, we conduct comprehensive experiments on three meta-learning problems, namely: (1) drug activity prediction, (2) pose prediction, and (3) image classification. We apply MetaMix on four gradient-based meta-learning algorithms, including MAML [7], MetaSGD [21], T-Net [20], and ANIL [32]. For comparison, we consider the following regularizers: Weight Decay as the traditional regularizer, CAVIA [52] and Meta-dropout [19] which regularizes the inner-loop, and MR-MAML [47] and TAML [15] both of which handle meta-generalization.

6.1 Drug Activity Prediction

Experimental Setup We solve a real-world application of drug activity prediction [26] where there are 4,276 target assays (i.e., tasks) each of which consists of a few drug compounds with tested activities against the target. We randomly selected 100 assays for meta-testing, 76 for meta-validation and the rest for meta-training. We repeat the random process four times and construct four groups of meta-testing assays for evaluation. Following [26], we evaluate the square of Pearson coefficient R^2 between the predicted $\hat{\mathbf{y}}_i^q$ and the groundtruth \mathbf{y}_i^q of all query samples for each i -the task, and report the mean and median R^2 values over all meta-testing assays as well as the number of assays with $R^2 > 0.3$ which is deemed as an indicator of reliability in pharmacology. We use a base model of two fully connected layers with 500 hidden units. In Beta(α, β), we set $\alpha = \beta = 0.5$. More details on the dataset and experimental settings are discussed in Appendix C.1.

Performance In practice, we notice that only updating the final layer in the inner-loop achieves the best performance, which is equivalent to ANIL. Thus, we apply this inner-loop update strategy to all baselines. For stability, here we also use ANIL++ [4] which stabilizes ANIL. In Table 2, we compare MetaMix with the baselines on the four drug evaluation groups. We observe that MetaMix consistently improves the performance despite of the backbone meta-learning algorithms (i.e., ANIL, ANIL++, MetaSGD, T-Net) in all scenarios. In addition, ANIL-MetaMix outperforms other anti-overfitting strategies. The consistent superior performance, even significantly better than the state-of-the-art pQSAR-max for this dataset, demonstrates that (1) MetaMix is compatible with

Table 2: Performance of drug activity prediction.

Model	Group 1			Group 2			Group 3			Group 4		
	Mean	Med.	>0.3									
pQSAR-max [26]	0.390	0.335	51	0.335	0.280	44	0.373	0.315	50	0.362	0.260	46
Weight Decay	0.307	0.228	40	0.243	0.157	34	0.259	0.171	38	0.290	0.241	47
CAVIA	0.300	0.232	42	0.234	0.132	35	0.260	0.184	39	0.317	0.292	46
Meta-dropout	0.319	0.203	41	0.250	0.172	35	0.281	0.214	39	0.316	0.275	47
MR-MAML	0.297	0.202	41	0.232	0.152	32	0.289	0.217	40	0.293	0.249	43
TAML	0.296	0.200	41	0.260	0.203	36	0.260	0.227	40	0.308	0.281	46
MetaSGD	0.331	0.224	45	0.249	0.187	33	0.282	0.226	40	0.312	0.287	48
T-Net	0.323	0.264	46	0.236	0.170	29	0.285	0.220	43	0.285	0.239	42
ANIL	0.299	0.184	41	0.226	0.143	30	0.268	0.199	37	0.304	0.282	48
ANIL++	0.367	0.299	50	0.315	0.252	43	0.335	0.289	48	0.362	0.324	51
MetaSGD-MetaMix	0.364	0.296	49	0.271	0.230	45	0.312	0.267	48	0.338	0.319	51
T-Net-MetaMix	0.352	0.291	50	0.276	0.229	42	0.310	0.285	47	0.336	0.298	50
ANIL-MetaMix	0.347	0.292	49	0.301	0.282	47	0.302	0.258	45	0.348	0.303	51
ANIL++-MetaMix	0.413	0.393	59	0.356	0.344	57	0.381	0.362	55	0.380	0.348	55

existing meta-learning algorithms; (2) MetaMix is capable of improving the meta-generalization ability. Furthermore, similar to Figure 2, we illustrate the predictive performance of the learned initialization after applying MetaMix in Figure 4 – MetaMix resolves the inconsistency and mitigates the overfitting issue on the query set, which empowers the meta-generalization capability enhanced.

Effect of Data Mixture Strategy To further investigate where the improvement stems from, we adopt six different mixup strategies for meta-training. The results of Group 3 and 4 are reported in Table 3 (see Appendix D.1 for results of Group 1 and 2). We use $\text{Mixup}(\mathcal{D}^m, \mathcal{D}^n)$ to denote the mixup of data \mathcal{D}^m and \mathcal{D}^n (e.g., $\text{Mixup}(\mathcal{D}^s, \mathcal{D}^q)$ in our case). $\mathcal{D}^{cob} = \mathcal{D}^s \oplus \mathcal{D}^q$ represents the concatenation of \mathcal{D}^s and \mathcal{D}^q . The fact that MetaMix enjoys better performance than $\text{Mixup}(\mathcal{D}^q, \mathcal{D}^q)$ suggests that MetaMix is much more than simple data augmentation, by addressing the inconsistency of the learned initialization across the support and query sets and thereby improving meta-generalization. In addition, involving the support set only is insufficient for meta-generalization due to its relative small gradient norm, which is further verified by the unsatisfactory performance of $\mathcal{D}^s \oplus \mathcal{D}^q$.

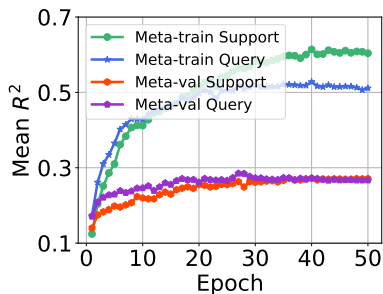


Figure 4: Optimization behavior of the initialization with MetaMix.

Table 3: Effect of mixture strategies on drug activity prediction.

Strategy	Group 3			Group 4		
	Mean	Med.	>0.3	Mean	Med.	>0.3
\mathcal{D}^q	0.335	0.289	48	0.362	0.324	51
$\text{Mixup}(\mathcal{D}^s, \mathcal{D}^s)$	0.214	0.154	29	0.191	0.141	22
$\text{Mixup}(\mathcal{D}^q, \mathcal{D}^q)$	0.341	0.306	50	0.358	0.325	53
$\mathcal{D}^{cob} = \mathcal{D}^s \oplus \mathcal{D}^q$	0.333	0.329	51	0.336	0.281	48
MetaMix	0.381	0.362	55	0.380	0.348	55

6.2 Pose Prediction

Experimental Setup Following [47], we use the multitask regression dataset created from Pascal 3D data [43], where an 128×128 grey-scale image is used as input and the orientation relative to a fixed pose labels each image. 50 and 15 objects are randomly selected for meta-training and meta-testing, respectively. The base model consists of a convolutional encoder and a decoder with four convolutional blocks. We set $\alpha = \beta = 0.5$ in $\text{Beta}(\alpha, \beta)$ (see Appendix C.2 for detailed settings).

Results Table 4 shows the performance (averaged MSE with 95% confidence interval) of baselines and MetaMix under 10-shot and 15-shot scenarios. The inner-loop regularizers are not as effective as MR-MAML and TAML in improving meta-generalization; MAML-MetaMix significantly improves MR-MAML, suggesting the effectiveness of bringing more data in than imposing meta-regularizers only. We also investigate the influence of mixup strategies on pose prediction in Appendix E.2, which again advocates the effectiveness of the proposed mixup strategy in recovering the true and unbiased model, as our theoretic analyses suggest. In Appendix E.1, we investigate the influence of different hyperparameter settings (e.g., α in $\text{Beta}(\alpha, \alpha)$), and demonstrate the robustness of MetaMix against different settings.

Table 4: Performance (MSE) of pose prediction

Model	10-shot	15-shot
Weight Decay	3.601 ± 0.095	3.327 ± 0.076
CAVIA	3.752 ± 0.105	3.286 ± 0.088
Meta-dropout	3.962 ± 0.098	3.621 ± 0.094
MR-MAML	3.565 ± 0.102	3.170 ± 0.092
TAML	3.597 ± 0.108	3.325 ± 0.096
ANIL	5.424 ± 0.134	5.316 ± 0.128
MAML	3.845 ± 0.098	3.324 ± 0.083
MetaSGD	3.813 ± 0.095	3.509 ± 0.081
T-Net	4.062 ± 0.104	3.632 ± 0.090
ANIL-MetaMix	5.207 ± 0.105	5.185 ± 0.086
MAML-MetaMix	3.312 ± 0.088	2.856 ± 0.070
MetaSGD-MetaMix	3.440 ± 0.083	2.839 ± 0.075
T-Net-MetaMix	3.837 ± 0.100	3.557 ± 0.085

6.3 Image Classification

Experimental Setup For image classification problems, standard benchmarks (e.g., Omniglot [18] and MiniImagenet [41]) are considered as mutually-exclusive tasks by introducing the shuffling mechanism of labels, which significantly alleviates the meta-overfitting issue [47]. To show the power of MetaMix, following [47], we adopt the non-mutually-exclusive setting for each image classification benchmark: each class with its classification label remains unchanged across different meta-training tasks during meta-training. Besides, we investigate image classification for heterogeneous tasks. We use the multi-dataset in [45] which consists of four subdatasets, i.e., Bird, Texture, Aircraft, and Fungi. The non-mutually-exclusive setting is also applied to this multi-dataset. Three representative heterogeneous meta-learning algorithms (i.e., MMAML [42], HSML [45], ARML [46]) are taken as baselines and applied with MetaMix. For each task, the classical N-way, K-shot setting is used to evaluate the performance. We use the standard four-block convolutional neural network as the base model. We set $\alpha = \beta = 2.0$ for all datasets. Detailed descriptions of experiment settings and hyperparameters are discussed in Appendix C.3.

Table 5: Performance (Accuracy) of image classification on Omniglot and MiniImagenet.

Model	Omniglot		MiniImagenet	
	20-way 1-shot	20-way 5-shot	5-way 1-shot	5-way 5-shot
Weight Decay	86.81 \pm 0.64%	96.20 \pm 0.17%	33.19 \pm 1.76%	52.27 \pm 0.96%
CAVIA	87.63 \pm 0.58%	94.16 \pm 0.20%	34.27 \pm 1.79%	50.23 \pm 0.98%
MR-MAML	89.28 \pm 0.59%	96.66 \pm 0.18%	35.00 \pm 1.60%	54.39 \pm 0.97%
Meta-dropout	85.60 \pm 0.63%	95.56 \pm 0.17%	34.32 \pm 1.78%	52.40 \pm 0.96%
TAML	87.50 \pm 0.63%	95.78 \pm 0.19%	33.16 \pm 1.68%	52.78 \pm 0.97%
MAML	87.40 \pm 0.59%	93.51 \pm 0.25%	32.93 \pm 1.70%	51.95 \pm 0.97%
MetaSGD	87.72 \pm 0.61%	95.52 \pm 0.18%	33.70 \pm 1.63%	52.14 \pm 0.92%
T-Net	87.71 \pm 0.62%	95.67 \pm 0.20%	33.73 \pm 1.72%	54.04 \pm 0.99%
ANIL	88.35 \pm 0.56%	95.85 \pm 0.19%	34.13 \pm 1.67%	52.59 \pm 0.96%
MAML-MetaMix	91.82 \pm 0.50%	97.63 \pm 0.15%	36.80 \pm 1.72%	57.55 \pm 1.01%
MetaSGD-MetaMix	93.48 \pm 0.59%	98.00 \pm 0.15%	38.86 \pm 1.65%	56.66 \pm 0.98%
T-Net-MetaMix	92.03 \pm 0.47%	97.66 \pm 0.16%	38.17 \pm 1.67%	58.57 \pm 0.96%
ANIL-MetaMix	90.78 \pm 0.58%	96.88 \pm 0.17%	37.23 \pm 1.72%	57.75 \pm 0.99%

Table 6: Performance (Accuracy) of image classification on Multi-dataset (see Appendix F.1 for accuracy with 95% confidence interval).

Model	5-way 1-shot				5-way 5-shot			
	Bird	Texture	Aircraft	Fungi	Bird	Texture	Aircraft	Fungi
MMAML	40.03%	25.43%	29.33%	31.13%	61.64%	34.76%	51.89%	44.48%
HSML	40.49%	26.40%	31.67%	30.43%	61.07%	35.48%	48.07%	43.42%
ARML	40.83%	27.03%	30.17%	30.66%	64.31%	36.11%	50.76%	46.11%
MMAML-MetaMix	44.99%	29.46%	35.13%	31.43%	63.85%	39.52%	59.29%	47.48%
HSML-MetaMix	43.83%	29.13%	34.71%	32.56%	65.38%	38.94%	55.19%	47.86%
ARML-MetaMix	44.20%	29.63%	34.03%	33.21%	65.96%	41.07%	58.02%	48.09%

Results In Table 5 and Table 6, we report the performance (accuracy with 95% confidence interval) on homogeneous datasets (i.e., Omniglot, MiniImagenet) and heterogeneous datasets, respectively. Aligned with other problems, in all non-mutually-exclusive datasets, applying the MetaMix strategy consistently improves existing meta-learning algorithms. For example, MAML-MetaMix significantly boosts MAML and most importantly outperforms MR-MAML, substantiating the effectiveness of MetaMix in improving the meta-generalization ability. It is worth mentioning that we also conduct the experiments on the standard mutually-exclusive setting of MiniImagenet in Appendix F.2. Though the label shuffling has significantly mitigated meta-overfitting, applying MetaMix still improves the meta-generalization to some extent. By varying mixup strategies in image classification of MiniImagenet in Table 7 (results of Omniglot are reported in Appendix F.3), we again corroborate our theoretic analysis that the knowledge distillation across support and query sets explains why MetaMix works. Besides, under the MiniImagenet 5-shot scenario, we investigate the influence of different hyperparameters, including sampling λ from the Beta distribution with different values of α and β , varying different fixed values of λ , and adjusting the layer to mixup (i.e., \mathcal{C} in Eqn. (4)) in Appendix F.4. All these studies indicate the robustness of MetaMix against hyperparameter settings.

Visualization of Decision Boundary In Figure 5 and Appendix F.5, we visualize the decision boundaries of MAML and MAML-MetaMix under the MiniImagenet 5-shot setting following [19]. We randomly select two classes for a meta-testing task and depict a binary decision boundary for the last layer of hidden representations. The figures show that the mixed samples by MetaMix do bridge the gap between support and query samples, and push the representations to be more compact (as we hypothesized in the end of Section 3) and the decision boundary to generalize better.

Table 7: Performance (Accuracy) of MiniImagenet w.r.t. different data mixture strategies.

Strategy	MiniImagenet	
	5-way 1-shot	5-way 5-shot
\mathcal{D}^q	$32.93 \pm 1.70\%$	$51.95 \pm 0.97\%$
Mixup($\mathcal{D}^s, \mathcal{D}^s$)	$24.39 \pm 1.48\%$	$33.18 \pm 0.82\%$
Mixup($\mathcal{D}^q, \mathcal{D}^q$)	$34.56 \pm 1.77\%$	$55.80 \pm 0.97\%$
$\mathcal{D}^{cob} = \mathcal{D}^s \oplus \mathcal{D}^q$	$33.33 \pm 1.70\%$	$51.97 \pm 0.96\%$
MetaMix	$36.80 \pm 1.72\%$	$57.55 \pm 1.01\%$

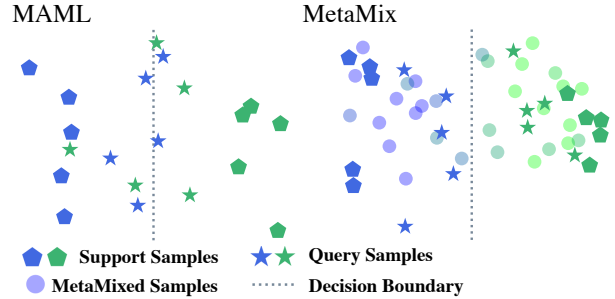


Figure 5: Visualization of decision boundaries of the last layer of hidden representations.

7 Conclusion

Current gradient-based meta-learning algorithms are at high risk of overfitting on meta-training tasks but poorly generalizing to meta-testing tasks. To address this issue, we propose a novel MetaMix strategy, which actively involves the support in the outer-loop optimization process. MetaMix linearly combines the input and associated hidden representations of support and target sets. We theoretically demonstrate that MetaMix can improve the meta-generalization capability. The state-of-the-art results in three different real-world datasets demonstrate the effectiveness and compatibility of MetaMix.

A Detailed Proof

In this section, we give the detailed proof of Section 4 in the original paper.

A.1 Proof of Lemma 1

We apply first and second-order Taylor expansion of \mathbf{g}_ϕ^q around θ_0 , and obtain the result as follows:

- First-order approximation:

$$\mathbf{g}_\phi^q = \mathbf{g}_{\theta_0}^q + \mathcal{O}(\mu) \quad (12)$$

- Second-order approximation:

$$\begin{aligned} \mathbf{g}_\phi^q &= \mathbf{g}_{\theta_0}^q + \mathbf{H}_{\theta_0}^q (\phi - \theta_0) + \mathcal{O}(\|\phi - \theta_0\|^2) \\ &= \mathbf{g}_{\theta_0}^q - \mu \mathbf{H}_{\theta_0}^q \mathbf{g}_{\theta_0}^s + \mathcal{O}(\mu^2) \end{aligned} \quad (13)$$

Recall the bi-level optimization process of MAML as:

$$\theta_0^* := \min_{\theta_0} \frac{1}{n_T} \sum_{i=1}^{n_T} [\mathcal{L}(f_{\phi_i}(\mathbf{X}_i^q), \mathbf{Y}_i^q)], \text{ s.t. } \phi_i = \theta_0 - \mu \nabla_{\theta} \mathcal{L}(f_{\theta}(\mathbf{X}_i^s), \mathbf{Y}_i^s). \quad (14)$$

By approximating the gradient of the loss in Eqn. (14) w.r.t. θ_0 using Eqns. (12) and (13), we have

$$\begin{aligned} \nabla_{\theta_0} \mathcal{L}(f_{\phi}(\mathbf{X}^q), \mathbf{Y}^q) &= (\mathbf{I} - \mu \mathbf{H}_{\theta_0}^s) \mathbf{g}_{\phi}^q \\ &= \mathbf{g}_{\phi}^q - \mu \mathbf{H}_{\theta_0}^s \mathbf{g}_{\phi}^q \\ &= \mathbf{g}_{\theta_0}^q - \mu \mathbf{H}_{\theta_0}^q \mathbf{g}_{\theta_0}^s - \mu \mathbf{H}_{\theta_0}^s \mathbf{g}_{\phi}^q + \mathcal{O}(\mu^2) \end{aligned} \quad (15)$$

$$= \mathbf{g}_{\theta_0}^q - \mu \mathbf{H}_{\theta_0}^q \mathbf{g}_{\theta_0}^s - \mu \mathbf{H}_{\theta_0}^s \mathbf{g}_{\theta_0}^q + \mathcal{O}(\mu^2) \quad (16)$$

$$= \mathbf{g}_{\theta_0}^q - \mu \nabla_{\theta} \langle \mathbf{g}_{\theta_0}^s, \mathbf{g}_{\theta_0}^q \rangle + \mathcal{O}(\mu^2), \quad (17)$$

where Eqn. (15) applies second-order approximation (i.e., Eqn. (13)); Eqn. (16) uses Eqn. (12) and the fact that $\mu \mathcal{O}(\mu) = \mathcal{O}(\mu^2)$; the last Eqn. (17) comes from the fact that $\mathbf{H}_{\theta_0}^s = \nabla \mathbf{g}_{\theta_0}^s$ and $\mathbf{H}_{\theta_0}^q = \nabla \mathbf{g}_{\theta_0}^q$.

A.2 Proof of Double Linear Loss Expansion

According to the properties of double linear loss $\mathcal{L}(f_{\theta}) = -\sum_j \mathbf{y}_j \ell^{\top}(f_{\theta}(\mathbf{x}_j))$ and the definition $\mathbf{z}_j = \ell^{\top}(f_{\theta}(\mathbf{x}_j))$, the double linear loss can be expanded as follows:

$$\begin{aligned} \mathcal{L}(f_{\theta_0}(\mathbf{X}^{mix}), \mathbf{Y}^{mix}) &= -\sum_j \mathbf{y}_j^{mix} \ell^{\top}(f_{\theta_0}(\mathbf{x}_j^{mix})) \\ &= -\sum_j (\lambda_j \mathbf{y}_j^s + (1 - \lambda_j) \mathbf{y}_j^q) \ell^{\top}(\lambda_j f_{\theta_0}(\mathbf{x}_j^s) + (1 - \lambda_j) f_{\theta_0}(\mathbf{x}_j^q)) \end{aligned} \quad (18)$$

$$= -\sum_j (\lambda_j \mathbf{y}_j^s + (1 - \lambda_j) \mathbf{y}_j^q) \left(\lambda_j \ell^{\top}(f_{\theta_0}(\mathbf{x}_j^s)) + (1 - \lambda_j) \ell^{\top}(f_{\theta_0}(\mathbf{x}_j^q)) \right) \quad (19)$$

$$= \sum_j \lambda_j^2 \mathcal{L}_j^s + (1 - \lambda_j)^2 \mathcal{L}_j^q - \lambda_j (1 - \lambda_j) (\mathbf{y}_j^s \mathbf{z}_j^{q\top} + \mathbf{y}_j^q \mathbf{z}_j^{s\top}), \quad (20)$$

where Eqn. (18) and Eqn. (19) come from the linearity of double linear loss $\mathcal{L}(f_{\theta})$ on \mathbf{x}_j and \mathbf{y}_j .

A.3 Proof and Analysis of the Least-square Regression Problem

In this part, we provide the full proof of Eqn. (11). Besides, we conduct an empirical study on the this problem via a simple one-dimension regression task. In this toy experiment, we set the groundtruth regression function as $y = 5x$, and generate the support set samples by randomly sampling x and setting $y = (5 + 0.3)x + \epsilon$ where $\epsilon \sim \mathcal{N}(0, 0.1)$ is some noise. The query set is generated in the same way, except that $y = (5 - 0.3)x + \epsilon$. The results in Figure 6 demonstrate that without MetaMix, the original one-step MAML simply overfits the query samples, which verifies our claim in Section 1. When integrating one-step MAML with MetaMix, the fitting curve nearly matches the curve of the groundtruth function, which demonstrates the effectiveness of MetaMix in improving the generalization.

The full proof of Eqn. (11) is detailed as follows.

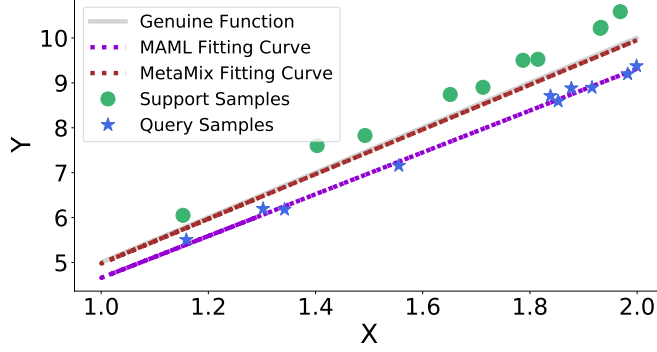


Figure 6: A toy case for least-square regression. The dashed lines represent the fitting curves for MAML (violet) and MetaMix (brown), respectively. The grey solid line denotes the groundtruth function.

Given $\mathcal{L}(f_\theta) = \sum_j \|\mathbf{y}_j - \theta^\top \mathbf{x}_j\|^2$ and $z_j = \mathbf{y}_j - \theta^\top \mathbf{x}_j$, we can derive that

$$\begin{aligned} \mathcal{L}(f_{\theta_0}(\mathbf{X}^{mix}), \mathbf{Y}^{mix}) &= \left\| \mathbb{E}_{\lambda \sim \text{Beta}(\alpha, \alpha)} [\lambda \mathbf{Y}^s + (\mathbf{I} - \lambda) \mathbf{Y}^q] - \theta^\top \mathbf{X} \right\|^2 \\ &= \sum_j \left\| \mathbb{E}_{\lambda_j \sim \text{Beta}(\alpha, \alpha)} \mathbb{E}_{z_j \sim \text{Ber}(\lambda_j)} [z_j \mathbf{y}_j^s + (1 - z_j) \mathbf{y}_j^q] - \theta^\top \mathbf{x}_j \right\|^2 \end{aligned} \quad (21)$$

$$= \sum_j \left\| \mathbb{E}_{z_j \sim \text{Ber}(0.5)} \mathbb{E}_{\lambda_j \sim \text{Beta}(\alpha + 1 - z_j, \alpha + z_j)} [z_j \mathbf{y}_j^s + (1 - z_j) \mathbf{y}_j^q] - \theta^\top \mathbf{x}_j \right\|^2 \quad (22)$$

$$= \sum_j \left\| \mathbb{E}_{z_j \sim \text{Ber}(0.5)} [z_j \mathbf{y}_j^s + (1 - z_j) \mathbf{y}_j^q] - \theta^\top \mathbf{x}_j \right\|^2 \quad (23)$$

$$= \left\| \frac{1}{2} \mathbf{Y}^s + \frac{1}{2} \mathbf{Y}^q - \theta^\top \mathbf{X} \right\|^2 \quad (24)$$

$$\begin{aligned} &= \left\| \left(\mathbf{w} + \mathbb{E} \left[\frac{\boldsymbol{\epsilon}^s + \boldsymbol{\epsilon}^q}{2} \right] \right)^\top \mathbf{X} - \theta^\top \mathbf{X} \right\|^2 \\ &= \|(\mathbf{w} - \theta)^\top \mathbf{X}\|^2, \end{aligned} \quad (25)$$

where Eqn. (21) is presented with the expectation of a Bernoulli variable; Eqn. (22) is rewritten by introducing the Bayes's rule $p(\lambda_j | z_j) p(z_j) = p(z_j | \lambda_j) p(\lambda_j)$ and applying the fact that the Beta distribution is the conjugate prior of the Bernoulli distribution; Eqn. (23) is based on the fact that λ does not exist in the equation and thus it does not affect the value of the equation; Eqn. (24) is updated with the expectation of a Bernoulli variable; Eqn. (25) comes from the fact $0 = \mathbb{E}[\boldsymbol{\epsilon}] = \frac{1}{2} \boldsymbol{\epsilon}^s + \frac{1}{2} \boldsymbol{\epsilon}^q$.

B Additional Information for MetaMix

B.1 Figure for the Beta Distribution

For the Beta(α, β) distribution, we illustrate both symmetric ($\alpha = \beta$) and skewed (i.e., $\alpha \neq \beta$) scenarios in Figure 7.

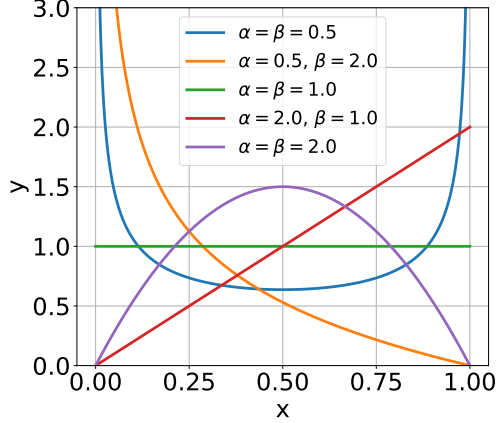


Figure 7: Illustration of the Beta Distribution. Here $\alpha = \beta$ and $\alpha \neq \beta$ represent the symmetric and skewed distributions, respectively.

B.2 Pseudo-codes

Take MAML-MetaMix as an example, we show the pseudo-codes for both meta-training and meta-testing in Alg. 1 and Alg. 2, respectively.

Algorithm 1 MAML-MetaMix in Meta-training

Require: Task distribution $p(\mathcal{T})$; Learning rate μ, η ; Beta distribution parameters α, β ; MetaMix candidate layer set \mathcal{C}

- 1: Randomly initialize parameter θ_0
 - 2: **while** not converge **do**
 - 3: Sample a batch of tasks $\{\mathcal{T}_i\}_{i=1}^n$
 - 4: **for all** \mathcal{T}_i **do**
 - 5: Sample support set $\mathcal{D}_i^s = \{(\mathbf{x}_{i,j}^s, \mathbf{y}_{i,j}^s)\}_{j=1}^{K^s}$ and query set $\mathcal{D}_i^q = \{(\mathbf{x}_{i,j}^q, \mathbf{y}_{i,j}^q)\}_{j=1}^{K^q}$ from \mathcal{T}_i
 - 6: Compute the task-specific parameter ϕ_i via the inner-loop gradient descent, i.e., $\phi_i = \theta_0 - \mu \nabla_{\theta} \mathcal{L}(f_{\theta}(\mathbf{X}_i^s), \mathbf{Y}_i^s)$
 - 7: Sample MetaMix parameter $\lambda \sim \text{Beta}(\alpha, \beta)$ and mixed layer l from \mathcal{C}
 - 8: Forward both support and query sets and mixed them at layer l as: $\mathbf{X}_{i,l}^{mix} = \lambda f_{\phi_i}(\mathbf{X}_i^s) + (\mathbf{I} - \lambda) f_{\phi_i}(\mathbf{X}_i^q)$, $\mathbf{Y}_i^{mix} = \lambda \mathbf{Y}_i^s + (\mathbf{I} - \lambda) \mathbf{Y}_i^q$
 - 9: Continual forward $\mathbf{X}_{i,l}^{mix}$ to the rest of layers and compute the loss as $\mathcal{L}(f_{\phi^{L-l}}(\mathbf{X}_{i,l}^{mix}), \mathbf{Y}_i^{mix})$
 - 10: **end for**
 - 11: Update $\theta_0 \leftarrow \theta_0 - \frac{1}{n} \sum_{i=1}^n \mathbb{E}_{\lambda \sim \text{Beta}(\alpha, \beta)} \mathbb{E}_{l \sim \mathcal{C}} [\mathcal{L}(f_{\phi^{L-l}}(\mathbf{X}_{i,l}^{mix}), \mathbf{Y}_i^{mix})]$
 - 12: **end while**
-

B.3 More Details for Singular Values

In total, we consider 30 tasks sampled under the MiniImagenet 5-shot setting. For each class of each task, we calculate its singular values by performing singular value decomposition (SVD) on the representations before the linear layer. The largest singular value for the first class is averaged over these 30 tasks and reported. Different algorithms, such as MAML, MetaMix, and MR-MAML included here, adapt each task to different models with different representations for SVD. We compare

Algorithm 2 MAML-MetaMix in Meta-testing

Require: Learning rate μ ; Optimized parameter θ_0^*

- 1: Compute the task-specific parameter ϕ_t as $\phi_t = \theta_0^* - \mu \nabla_{\theta} \mathcal{L}(f_{\theta}(\mathbf{X}_t^s), \mathbf{Y}_t^s)$
 - 2: Predict $\hat{\mathbf{Y}}_t^q$ on the query set \mathcal{D}_t^q
 - 3: Evaluate the performance via predicted value $\hat{\mathbf{Y}}_t^q$ and actual value \mathbf{Y}_t^q
-

the average largest singular values by different algorithms and report the full results in Table 8. The results show that MetaMix reduces the largest singular value and achieves compact representations, which explains the improvement of the meta-generalization.

Table 8: Comparison of the average largest singular values by different algorithms for each class under the MiniImagenet 5-shot setting (full results).

Class	C1	C2	C3	C4	C5
MAML	29.81 ± 0.65	29.03 ± 0.66	29.74 ± 0.65	29.07 ± 0.74	28.83 ± 0.69
MR-MAML	23.42 ± 0.77	21.83 ± 0.98	22.72 ± 1.10	22.33 ± 0.93	22.31 ± 1.02
MetaMix	19.43 ± 0.45	18.84 ± 0.58	19.52 ± 0.63	19.79 ± 0.55	18.69 ± 0.45

C Detailed Experimental Setup

In this section, we provide more details on the experimental setup of our paper. All experiments are run on a GPU cluster and implemented by Tensorflow [1]. In the next, we discuss the setup for all the problems, including drug activity prediction, pose prediction, and image classification.

C.1 Drug Activity Prediction

For drug activity prediction, we use the publicly available dose-response activity assays from ChEMBL¹ and preprocessed in [26]. All 4,276 assays, as 4,276 tasks, are accessible and downloadable from this site². In each assay, there are a few training drug compounds with biologically tested activities against the target protein in this assay, as well as several testing compounds. The split of training and testing compounds follows the realistic split in [26]. The number of drug compounds varies from assay to assay, with an median of only 70 drug compounds per assay. To describe each compound, we follow [26] to use 1,024 dimensional Morgan fingerprint implemented in RDkit³. As mentioned in the experimental section in the main text, we randomly take 100 assays as meta-testing assays, and 76 assays for meta-validation and the rest of 4100 assays for meta-training. Here we report the assay IDs that belong to meta-validation and meta-testing, respectively, for all the four groups. Note that due to space limit we do not report the assay IDs for meta-training, which can be easily obtained by deducting the meta-validation and meta-testing assays from all 4276 assays.

- **Group 1**

¹<https://www.ebi.ac.uk/chembl>

²<https://pubs.acs.org/doi/10.1021/acs.jcim.9b00375#i21>

³<http://rdkit.org/>

- *Meta-validation*: 972800, 688641, 610565, 1536390, 211079, 1625735, 1641357, 688654, 1641103, 457234, 450707, 195220, 1366808, 49308, 924, 49312, 828065, 737313, 1528100, 596645, 1641767, 1535401, 688427, 969260, 453677, 978479, 1641008, 574385, 911154, 446257, 878513, 1640955, 902584, 1276473, 752567, 306492, 736957, 1640384, 1454018, 2755, 579907, 1527622, 761927, 89542, 809158, 978889, 556876, 478840, 688464, 1330005, 144341, 1528791, 1301597, 1641310, 209245, 608993, 1528801, 89064, 1527913, 4202, 688616, 1513, 510189, 1641197, 1527791, 688495, 89839, 1641201, 1528688, 752371, 688379, 938230, 596087, 835704, 566779, 688767.
- *Meta-testing*: 752640, 972801, 737284, 954885, 1528837, 1587725, 1527823, 1640977, 157713, 1285138, 1437208, 1349151, 1592870, 93228, 465460, 954934, 84556, 1567308, 1577550, 1285709, 654928, 620647, 864364, 575603, 1280627, 688257, 1443970, 1527947, 737424, 201877, 1457820, 603293, 809120, 883875, 1641128, 1534634, 1641655, 955073, 954571, 736971, 577227, 45264, 455393, 728290, 688357, 1301747, 105205, 865015, 665348, 820998, 759559, 1301769, 609034, 80649, 1641240, 965916, 34078, 1470241, 1348900, 333106, 1527607, 954703, 1641298, 1641300, 727385, 304989, 981861, 212325, 756584, 331630, 473976, 63356, 51590, 1640328, 954762, 1642379, 1527698, 1527704, 543133, 954781, 1301405, 619939, 605612, 585134, 1433006, 934321, 1642435, 1637320, 936907, 54735, 70610, 1508820, 1292758, 104407, 992729, 199642, 160234, 1528304, 629753, 931327.

• **Group 2**

- *Meta-validation*: 7296, 1276546, 87173, 688645, 1350406, 955016, 697223, 1163, 201739, 809231, 1528850, 1528212, 752533, 971798, 954388, 1626011, 1528480, 501795, 1527972, 470053, 1640867, 809128, 737064, 1642538, 954282, 978478, 786095, 29233, 1642418, 737075, 1536179, 1641399, 1527735, 609465, 1640506, 1641659, 307259, 1537597, 769089, 140229, 789189, 860488, 766795, 48587, 1528909, 1451727, 219472, 737105, 955090, 311637, 1528022, 1632983, 727385, 1456602, 1641179, 688347, 67039, 434528, 1564001, 727521, 688483, 595939, 1436004, 736997, 1528160, 1640426, 4202, 102381, 45422, 1641073, 47858, 37363, 1641720, 688889, 1301756, 556797.
- *Meta-testing*: 835072, 539657, 1641997, 1639955, 1638422, 1639959, 1622038, 637980, 28188, 91168, 954915, 425511, 688685, 155185, 39493, 155208, 1641035, 1288277, 755797, 954462, 812132, 87656, 1536113, 48248, 744057, 210045, 1642144, 50337, 325795, 1527974, 1642150, 814256, 1641143, 438974, 217297, 1641170, 688340, 1641688, 688357, 649964, 930033, 447747, 566532, 1641737, 49425, 562451, 817939, 688403, 817944, 52506, 452895, 984872, 311595, 899888, 646978, 1642307, 664904, 1641802, 1466703, 1466704, 809297, 147797, 1640791, 305497, 209245, 603488, 701282, 752485, 302952, 122731, 563052, 1561972, 1528692, 1642361, 1528698, 737150, 1301374, 51590, 364426, 1642378, 899993, 752538, 1640355, 1446827, 62394, 842684, 1640893, 44489, 688589, 208335, 1642449, 858065, 1640919, 1528791, 1528294, 1520, 1640952, 92156, 63997, 69119.

• **Group 3**

- *Meta-validation*: 856700, 688641, 448646, 1613063, 1301767, 624014, 559247, 1527953, 1640339, 49558, 737046, 809242, 1642522, 1641371, 1527965, 592925, 954655, 688416, 305569, 538786, 1535011, 208672, 1592863, 688550, 1527974, 1527976, 1642272, 305065, 809259, 1640189, 96941, 688685, 954799, 978480, 934321, 1637168, 29233, 45236, 306221, 1535033, 1640506, 1290683, 158524, 936637, 647615, 422463, 1459648, 1640904, 954953, 1361352, 654923, 1641164, 954959, 1301583, 688210, 1508820, 45272, 688346, 737371, 162397, 775393, 535396, 1301477, 4197, 651627, 75756, 3819, 737391, 1641201, 1528692, 1294964, 456311, 737273, 1301756, 1640573, 42878.
- *Meta-testing*: 688643, 688645, 159749, 1527820, 539663, 303638, 1638422, 954399, 330271, 70695, 1295917, 1642542, 1527862, 1528890, 200254, 540741, 1365575, 761928, 688201, 37966, 1537108,

336476, 511069, 1301599, 1528416, 206959, 478840, 1503357, 1642117, 1536654, 688274, 1527963, 688288, 688293, 688816, 745138, 438974, 88771, 459971, 714443, 1289425, 1451729, 1284820, 954602, 954604, 208118, 198910, 809216, 610565, 1528071, 453897, 770827, 216843, 828171, 306447, 562451, 1642271, 1528097, 28965, 367910, 1642296, 1528125, 1528145, 1555281, 49489, 493905, 876885, 1290079, 468834, 1528677, 756582, 1338728, 1528170, 845165, 1528696, 617338, 1301888, 102785, 1527682, 940424, 1528724, 809380, 1446827, 864186, 1291714, 642499, 688586, 1513931, 32721, 954834, 1536468, 688598, 1556442, 901084, 954845, 1527780, 1640932, 477677, 829947, 1528829.

- **Group 4**

- *Meta-validation*: 688391, 1641992, 1641737, 306314, 311816, 813068, 68748, 1536775, 823822, 1639955, 696215, 1469079, 971801, 41884, 637980, 1298461, 76063, 688416, 1637151, 619938, 1642274, 885155, 572966, 510887, 1641000, 1528488, 954411, 1642415, 138287, 1527985, 56498, 27571, 458930, 311855, 809146, 307259, 950588, 736957, 1527742, 809152, 592450, 809156, 1528648, 954957, 209231, 490576, 1528273, 1641170, 45265, 1528917, 1528149, 1292759, 809175, 53367, 737370, 822749, 154333, 67039, 737273, 1640162, 737379, 763492, 809193, 954987, 104172, 510189, 1528695, 208754, 688243, 45044, 954482, 1640307, 1528183, 1642489, 1527674, 688254.
- *Meta-testing*: 1556484, 688644, 737290, 1301520, 1642001, 1528850, 688661, 971799, 1642520, 46624, 1537067, 1641005, 1641010, 688185, 954938, 443966, 599616, 439367, 1537607, 954956, 688719, 615506, 654934, 1589851, 104542, 457824, 1641573, 1527916, 737391, 1301619, 211078, 52874, 955024, 32404, 158358, 566940, 50848, 1527970, 1349288, 1586856, 860330, 688818, 1536181, 48316, 491718, 1296583, 954567, 1566412, 66255, 66267, 809183, 425699, 467683, 464617, 752377, 508163, 872708, 1640197, 1301765, 809221, 809239, 1528102, 809255, 1536298, 1640747, 688431, 1636657, 213817, 1466703, 1301330, 1545042, 737622, 1452895, 950625, 856937, 493931, 954743, 809346, 558984, 1642378, 591251, 1640852, 305050, 934299, 1640862, 1640351, 1642418, 558515, 1511354, 1330619, 1528770, 1291715, 901575, 1640904, 1439182, 1537998, 737235, 1301469, 37371, 797692.

The base model of drug activity prediction is a two-layer Multilayer Perceptron(MLP) neural network with 500 neurons in each layer. Each fully connected layer is followed by a batch normalization layer and leaky ReLU activation (negative slope is 0.01). In Beta(α, α), we set $\alpha = 0.5$. We set the candidate layer \mathcal{C} as layer 1 and layer 2. During meta-training, the task batch size, the outer-loop learning rate, the inner-loop learning rate are set to 8, 0.001, and 0.01, respectively. The meta-training process altogether runs for 50 epochs, each of which includes 500 iterations. In either meta-training or meta-testing, the number of inner-loop adaptation steps equals to 5.

C.2 Pose Prediction

In the pose prediction problem, we follow [47] to preprocess the pose tasks⁴. The meta-training and meta-testing include 50 and 15 categories, respectively, where each category contains 100 gray images in the size of 128×128 . The meta-training and meta-testing categories are listed as follows.

- **Meta-training Categories**: tvmonitor-03, tvmonitor-01, tvmonitor-02, bus-06, bus-05, bus-04, bus-02, bicycle-06, bicycle-05, bicycle-03, bicycle-01, boat-06, boat-03, boat-04, boat-01, boat-02, diningtable-06, diningtable-05, diningtable-04, diningtable-01, diningtable-02, aeroplane-06,

⁴code link: https://github.com/google-research/google-research/tree/master/meta_learning_without_memorization/pose_data

aeroplane-04, aeroplane-01, aeroplane-02, chair-10, chair-08, chair-06, chair-05, chair-03, chair-07, chair-04, chair-01, chair-02, sofa-06, sofa-05, sofa-04, sofa-02, motorbike-05, motorbike-03, motorbike-04, motorbike-01, motorbike-02, car-10, car-08, car-06, car-05, car-03, car-07, car-04, car-01, car-02.

- **Meta-testing Categories:** tvmonitor-04, bus-03, bus-01, bicycle-04, bicycle-02, boat-05, diningtable-03, aeroplane-08, aeroplane-05, aeroplane-03, aeroplane-07, chair-09, sofa-03, sofa-01, car-09.

In pose prediction, the base model is comprised of a fixed encoder and an adapted decoder. Each convolutional block is composed of a convolutional layer, a batch normalization layer and a ReLU activation layer. During the inner-loop optimization, we fix the encoder and only update the parameters in the decoder (i.e., the encoder layers are only meta-updated in the outer-loop optimization). For the hyperparameters in pose prediction, both inner-loop and outer-loop learning rates are set as 0.01. In addition, we set the hyperparameter α in the Beta distribution as 0.5 and the number of adaptation steps in the inner-loop optimization as 5. The candidate set \mathcal{C} for mixup is set to include the input layer (layer 0) as well as all hidden layers (i.e., layer 1, layer 2, and layer 3). All hyperparameters are selected according to the performance on the meta-validation set (10 categories), which are randomly selected from the meta-training categories.

C.3 Image Classification

In image classification, the image sizes of Omniglot, MiniImagenet, Multi-dataset are set to be $28 \times 28 \times 1$, $84 \times 84 \times 3$ and $84 \times 84 \times 3$, respectively. Under the non-mutually exclusive setting, taking 5-way miniImagenet as an example, 64 meta-training classes are split to 5 sets, where 4 sets have 13 classes and the rest one has 12 classes. For each set, a fixed class label is assigned to each class within this set, which remains unchanged across different tasks. During meta-training, we randomly select one class from each set and take all the five selected classes to construct a task, which ensures that each class consistently has one label across tasks. In our experiments, we list the classes within each set as follows.

- **Set 1:** n07584110, n04243546, n03888605, n03017168, n04251144, n02108551, n02795169, n03400231, n03476684, n04435653, n02120079, n01910747, n03062245
- **Set 2:** n03347037, n04509417, n03854065, n02108089, n04067472, n04596742, n01558993, n04612504, n02966193, n07697537, n01843383, n03838899, n02113712
- **Set 3:** n04604644, n02105505, n02108915, n03924679, n01704323, n09246464, n04389033, n03337140, n06794110, n04258138, n02747177, n13054560, n04443257
- **Set 4:** n13133613, n01770081, n02606052, n02687172, n02101006, n03676483, n04296562, n02165456, n04515003, n01749939, n02111277, n02823428, n01532829
- **Set 5:** n02091831, n07747607, n03998194, n02089867, n02074367, n02457408, n04275548, n03220513, n03527444, n03908618, n03207743, n03047690

A similar process is applied to Omniglot, where 1200 meta-training classes are randomly split into 20 sets with 60 classes in each set. In Multi-dataset, each subdataset is split into 5 sets. In the subdatasets Bird, Aircraft and Fungi, we have 4 sets each of which includes 13 classes while the rest one includes 12. In the subdataset Texture, however, each set contains 6 classes.

For all datasets, we utilize the classical convolutional neural network with 4 convolutional blocks as the base model [7, 35]. It is worth to mention that [47] adopts a deeper network as the base model under the non-mutually exclusive setting. The deeper network includes 3 convolutional layers with a fully connected layer as the encoder and 3 convolutional decoder layers, where the encoder is fixed during inner-loop optimization. In our practice, the shallower network achieves better performance in all meta-learning algorithms, as a result of more serious overfitting issues caused by the deeper network. In Table 9, we illustrate the comparison of pre inner-update accuracy and meta-testing post inner-update accuracy during meta-training under the Omniglot 20-way, 1-shot setting, where MAML, MR-MAML are included as baselines. The results indicate that the deeper structure is easier to memorize all data samples via the learned initialization; therefore, we adopt the shallow network (i.e., standard 4-block convolutional layers) in this experiment.

Table 9: Comparison between the shallow and deeper base model under the Omniglot 20-way 1-shot setting.

Methods	Meta-training Pre-update		Meta-testing Post-update	
	Shallow	Deep	Shallow	Deep
MAML	$14.38 \pm 0.40\%$	$98.59 \pm 0.05\%$	$87.40 \pm 0.59\%$	$8.82 \pm 0.42\%$
MR-MAML	$5.63 \pm 0.36\%$	$5.12 \pm 0.34\%$	$89.28 \pm 0.59\%$	$83.75 \pm 0.67\%$

For hyperparameter settings, in both MiniImagenet and Multi-dataset, the inner-loop learning rate μ and the outer-loop learning rate η are set as 0.01, 0.001, respectively. In Omniglot, μ and η are set as 0.1, 0.005, respectively. The hyperparameter α of the Beta distribution $\text{Beta}(\alpha, \alpha)$ is set as 2.0 for all datasets. Besides, the candidate layer set \mathcal{C} for both MiniImagenet and Multi-dataset is set as layer (0, 1, 2, 3). In Omniglot, the candidate set \mathcal{C} is set as layer (1, 2, 3). All hyperparameters are determined by the performance on the meta-validation set.

D Additional Results for Drug Activity Prediction

D.1 Additional Results of Mixup Strategies on Group 1, 2

In the main text, we have reported the results of different mixup strategies on Group 3 and 4. Here we also report those on Group 1 and 2. Similar to the conclusion drawn in Group 3 and 4, the results in Group 1 and 2 signify that MetaMix achieves the best performance over all mixup strategies.

Table 10: Effect of mixup strategies on Group 1 and 2 for drug activity prediction.

Strategies	Group 1			Group 2		
	Mean	Med.	>0.3	Mean	Med.	>0.3
\mathcal{D}^q	0.367	0.299	50	0.315	0.252	43
Mixup($\mathcal{D}^s, \mathcal{D}^s$)	0.224	0.164	33	0.210	0.164	31
Mixup($\mathcal{D}^q, \mathcal{D}^q$)	0.388	0.354	55	0.341	0.328	53
$\mathcal{D}^{cob} = \mathcal{D}^s \oplus \mathcal{D}^q$	0.376	0.324	52	0.301	0.242	44
MetaMix	0.413	0.393	59	0.356	0.344	57

D.2 Hyperparameter Analysis on Drug Activity Prediction

D.2.1 Analysis of the Candidate Layer Set \mathcal{C}

We further analyze the effect of different candidate layer sets \mathcal{C} on drug activity prediction. The results are reported in Table 11. Compared with $\mathcal{C} = 2$, $\mathcal{C} = 1$ leads to higher performances, suggesting that mixing low-level representations with the resulting compactness contributes more to the overall improvement. Furthermore, mixing all layers (i.e., $\mathcal{C} = (1, 2)$) achieves the best performance, indicating the necessity of jointly mixing the representations in all levels.

Table 11: Effect of the candidate layer set \mathcal{C} in MetaMix.

Mixed layers \mathcal{C}	Group 1			Group 2			Group 3			Group 4		
	Mean	Med.	>0.3	Mean	Med.	>0.3	Mean	Med.	>0.3	Mean	Med.	>0.3
(1)	0.412	0.362	59	0.333	0.328	53	0.355	0.318	51	0.390	0.349	56
(2)	0.405	0.324	51	0.324	0.256	44	0.354	0.304	50	0.387	0.353	57
(1,2)	0.413	0.393	59	0.356	0.344	57	0.381	0.362	55	0.380	0.348	55

D.2.2 Analysis of the Mixup Ratio

In MetaMix, the mixup ratio for the support and the query sets are controlled by the parameter λ , which is sampled from the Beta distribution $\text{Beta}(\alpha, \alpha)$. Here, we analyze the performance w.r.t. the change of mixup ratio. Specifically, we conduct two experiments: (1) we analyze the performance concerning the change of hyperparameter α ; (2) we fix the mixup ratio λ without being sampled from the Beta distribution. The results for the experiments (1) and (2) are shown in Figure 8 and Figure 9, respectively. In the analysis of α , though the overall performance is slightly better when $\alpha = 0.5$, our MetaMix strategy is still robust and not very sensitive to the shape of Beta distribution (i.e., different α). The conclusion is further strengthened by the analysis of fixed λ in Figure 9, where the performance remains relative stable between $\lambda \in [0.4, 0.75]$.

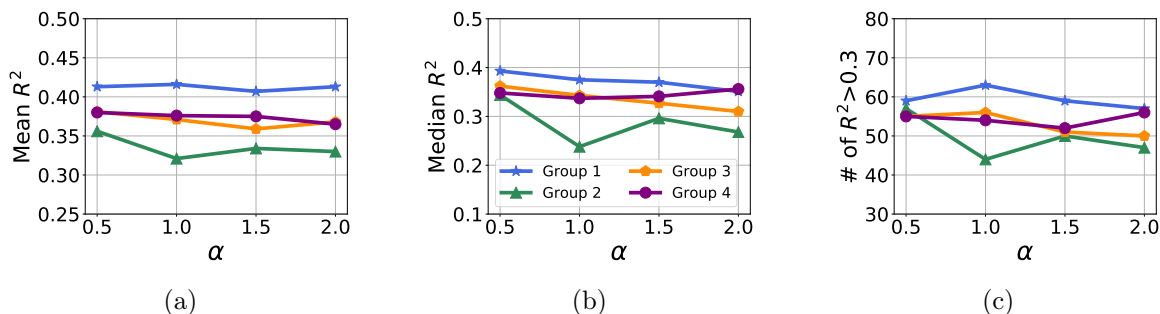


Figure 8: Performance on drug activity prediction w.r.t. the change of α in $\text{Beta}(\alpha, \alpha)$. The three subfigures (a), (b), (c) represent the results under different evaluation metrics.

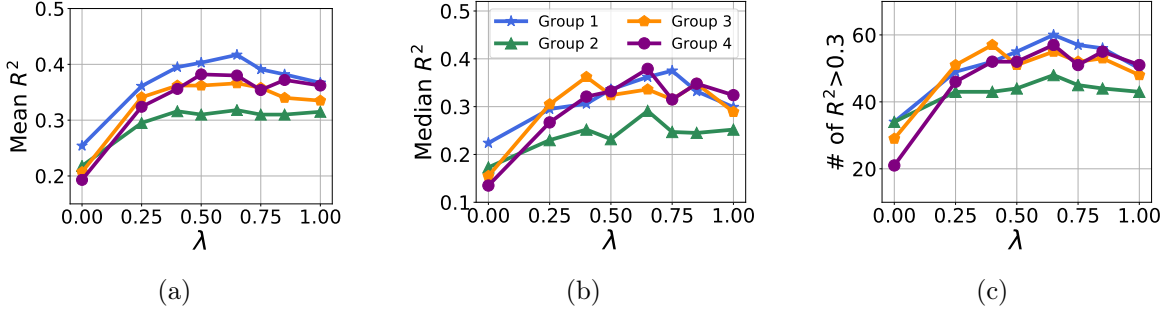


Figure 9: Performance w.r.t. the fixed λ in MetaMix (i.e., $\lambda f_{\phi_i^s}(\mathbf{X}_i^s) + (\mathbf{I} - \lambda) f_{\phi_i^q}(\mathbf{X}_i^q)$). The three subfigures (a), (b), (c) show the performance under different evaluation metrics (i.e. mean R^2 , median R^2 , the number of assays with $R^2 > 0.3$).

E Additional Results for Pose Prediction

E.1 Hyperparameter Analysis on Pose Prediction

E.1.1 Analysis of the Candidate Layer Set \mathcal{C}

Table 12 reports the performance w.r.t. the change of the mixup layer set \mathcal{C} . Though including the input layer, i.e., layer 0, slightly hurts the performance in some cases, MetaMix remains relative stable with different mixup layer sets \mathcal{C} .

Table 12: Performance (Accuracy) w.r.t. MetaMix candidate layer set \mathcal{C} under Pose 15-shot setting.

$ \mathcal{C} = 1$	Performance	$ \mathcal{C} = 2$	Performance	$ \mathcal{C} = 3$	Performance	$ \mathcal{C} = 4$	Performance
(0)	3.043 ± 0.081	(0,1)	2.969 ± 0.078	(0,1,2)	2.898 ± 0.079	(0,1,2,3)	2.856 ± 0.070
(1)	2.894 ± 0.073	(0,2)	2.888 ± 0.075	(0,1,3)	2.999 ± 0.078	-	-
(2)	2.922 ± 0.075	(0,3)	2.904 ± 0.080	(0,2,3)	3.067 ± 0.083	-	-
(3)	2.903 ± 0.072	(1,2)	2.870 ± 0.078	(1,2,3)	2.891 ± 0.077	-	-
-	-	(1,3)	2.883 ± 0.076	-	-	-	-
-	-	(2,3)	2.872 ± 0.071	-	-	-	-

E.1.2 Analysis of the Mixup Ratio

In pose prediction, we analyze the mixup ratio by investigating the performance w.r.t. the changes of two key parameters: (1) α in Beta(α, α); (2) the mixup ratio λ in $\mathbf{X}_{i,l}^{mix} = \lambda f_{\phi_i^s}(\mathbf{X}_i^s) + (\mathbf{I} - \lambda) f_{\phi_i^q}(\mathbf{X}_i^q)$. We show the results of α and λ in Figure 10a and Figure 10b, respectively. The stability of performance w.r.t. α and the stable region [0.4, 0.75] in the analysis of λ indicate the robustness of MetaMix under different Beta distribution shapes.

E.2 Effect of Mixup Strategies on Pose Prediction

In pose prediction, the performance w.r.t. different mixup strategies are reported in Table 13. The superiority of MetaMix over other strategies corroborates our theoretical analysis that MetaMix benefits the recovery of the biased model, which further improves the meta-generalization.

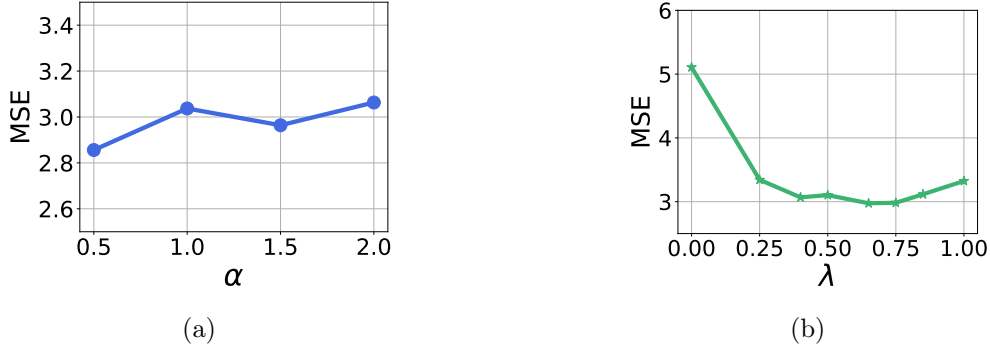


Figure 10: Performance w.r.t. (a) α in $\text{Beta}(\alpha, \alpha)$, and (b): the fixed mixup ratio λ under 15-shot pose prediction.

Table 13: Performance (MSE) of pose prediction w.r.t. different mixup strategies

Setting	\mathcal{D}^q	Mixup($\mathcal{D}^s, \mathcal{D}^s$)	Mixup($\mathcal{D}^q, \mathcal{D}^q$)	\mathcal{D}^{cob}	MetaMix
10-shot	3.845 ± 0.098	6.434 ± 0.100	3.694 ± 0.095	3.580 ± 0.089	3.312 ± 0.088
15-shot	3.324 ± 0.083	4.956 ± 0.084	3.265 ± 0.079	3.309 ± 0.082	2.856 ± 0.070

F Additional Results for Image Classification

F.1 Additional Results on Multi-dataset

In Table 14, we report the additional results (accuracy with 95% confidence interval) on Multi-datasets.

Table 14: Accuracy with 95% confidence interval on Multi-dataset.

Setting	Model	Bird	Texture	Aircraft	Fungi
5-way 1-shot	MMAML	$40.03 \pm 1.87\%$	$25.43 \pm 1.61\%$	$29.33 \pm 1.69\%$	$31.13 \pm 1.63\%$
	HSML	$40.49 \pm 1.78\%$	$26.40 \pm 1.66\%$	$31.67 \pm 1.68\%$	$30.43 \pm 1.66\%$
	ARML	$40.83 \pm 1.81\%$	$27.03 \pm 1.63\%$	$30.17 \pm 1.67\%$	$30.66 \pm 1.61\%$
	MMAML-MetaMix	$44.99 \pm 1.77\%$	$29.46 \pm 1.69\%$	$35.13 \pm 1.66\%$	$31.43 \pm 1.66\%$
	HSML-MetaMix	$43.83 \pm 1.68\%$	$29.13 \pm 1.67\%$	$34.71 \pm 1.71\%$	$32.56 \pm 1.67\%$
	ARML-MetaMix	$44.20 \pm 1.78\%$	$29.63 \pm 1.65\%$	$34.03 \pm 1.68\%$	$33.21 \pm 1.69\%$
5-way 5-shot	MMAML	$61.64 \pm 0.96\%$	$34.76 \pm 0.80\%$	$51.89 \pm 0.93\%$	$44.48 \pm 0.96\%$
	HSML	$61.07 \pm 1.04\%$	$35.48 \pm 0.83\%$	$48.07 \pm 0.91\%$	$43.42 \pm 0.94\%$
	ARML	$64.31 \pm 0.99\%$	$36.11 \pm 0.83\%$	$50.76 \pm 0.97\%$	$46.11 \pm 0.95\%$
	MMAML-MetaMix	$63.85 \pm 0.92\%$	$39.52 \pm 0.85\%$	$59.29 \pm 0.88\%$	$47.48 \pm 0.97\%$
	HSML-MetaMix	$65.38 \pm 0.96\%$	$38.94 \pm 0.81\%$	$55.19 \pm 0.90\%$	$47.86 \pm 0.96\%$
	ARML-MetaMix	$65.96 \pm 0.94\%$	$41.07 \pm 0.79\%$	$58.02 \pm 0.93\%$	$48.09 \pm 0.98\%$

F.2 Results under Mutually-exclusive Setting

In Table 15, we report the results under the standard mutually-exclusive setting on MiniImagenet. Under the mutually-exclusive setting, the mechanism of label shuffling is introduced to construct meta-training tasks, which significantly alleviates the meta-overfitting issue. However, applying MetaMix on this setting still achieves comparable or even better performance than original MAML, which further demonstrates the effectiveness of MetaMix to improve meta-generalization.

Table 15: Performance (Accuracy) of MiniImagenet under the mutually-exclusive setting.

Model	MiniImagenet	
	5-way 1-shot	5-way 5-shot
MAML	48.70 ± 1.84%	63.11 ± 0.92%
MAML-MetaMix	50.02 ± 1.83%	64.13 ± 0.95%

F.3 Effect of Mixup Strategies on Omniglot

Table 16 shows the effect of different mixup strategies on Omniglot dataset. Similar to the performance and conclusion on MiniImagenet, in Omniglot, MetaMix also enjoys the best performance compared with other mixup strategies.

Table 16: Performance (Accuracy) of Omniglot w.r.t. different data mixture strategies.

Strategies	Omniglot	
	20-way 1-shot	20-way 5-shot
\mathcal{D}^q	87.40 ± 0.59%	93.51 ± 0.25%
Mixup($\mathcal{D}^s, \mathcal{D}^s$)	46.98 ± 0.92%	85.56 ± 0.28%
Mixup($\mathcal{D}^q, \mathcal{D}^q$)	90.65 ± 0.56%	96.90 ± 0.16%
$\mathcal{D}^{cob} = \mathcal{D}^s \oplus \mathcal{D}^q$	86.74 ± 0.54%	95.54 ± 0.19%
MetaMix	91.53 ± 0.53%	97.63 ± 0.15%

F.4 Hyperparameter Analysis

F.4.1 Analysis of the Candidate Layer Set \mathcal{C}

In Table 17, we analyze the effect of the candidate layer set \mathcal{C} and report the performance under the 5-shot MiniImagenet scenario. The results indicate the robustness of MetaMix under different candidate layer sets, and we conclude that involving all layers achieves the best performance.

F.4.2 Analysis of the Mixup Ratio and the Skewed Beta Distribution

Under the Omniglot and MiniImagenet 5-shot setting, we further investigate the effect of key hyperparameters for mixup (i.e., α and λ). The results of MiniImagenet and Omniglot are shown

Table 17: Performance (Accuracy) w.r.t. the mixup layer set \mathcal{C} under the MiniImagenet 5-shot scenario.

$ \mathcal{C} = 1$	Performance	$ \mathcal{C} = 2$	Performance	$ \mathcal{C} = 3$	Performance	$ \mathcal{C} = 4$	Performance
(0)	$56.81 \pm 1.02\%$	(0,1)	$57.30 \pm 0.99\%$	(0,1,2)	$56.64 \pm 1.01\%$	(1,2,3,4)	$57.55 \pm 1.01\%$
(1)	$56.12 \pm 0.98\%$	(0,2)	$57.26 \pm 1.00\%$	(0,1,3)	$56.17 \pm 1.00\%$	-	-
(2)	$56.59 \pm 0.97\%$	(0,3)	$57.42 \pm 0.96\%$	(0,2,3)	$56.68 \pm 0.98\%$	-	-
(3)	$56.09 \pm 1.00\%$	(1,2)	$56.62 \pm 0.99\%$	(1,2,3)	$56.93 \pm 0.94\%$	-	-
-	-	(1,3)	$56.78 \pm 0.98\%$	-	-	-	-
-	-	(2,3)	$56.64 \pm 0.97\%$	-	-	-	-

in Figure 11. Similar to the previous analysis on drug activity prediction and pose prediction, the stability of performance w.r.t. α and the stable region in λ analysis demonstrate the robustness of MetaMix. The conclusion is further supported by the analysis of skewed Beta distribution (i.e., $\alpha \neq \beta$), whose results under the MiniImagenet 5-shot setting are reported in Table 18.

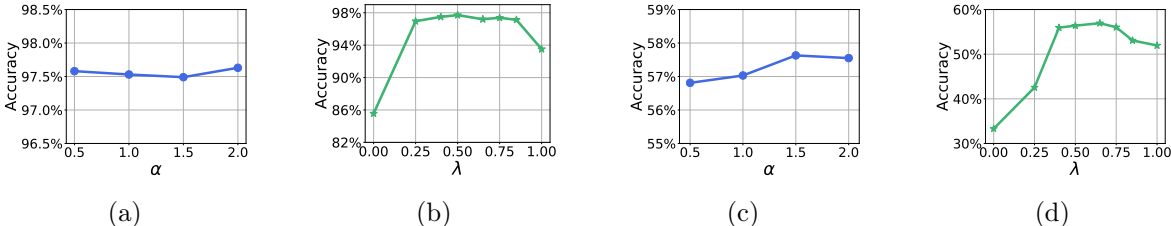


Figure 11: Performance w.r.t. (a)(c) α in $\text{Beta}(\alpha, \alpha)$ distribution; (b)(d) mixup ratio λ . (a)(b) show the results under the Omniglot 20-way, 5-shot setting; (c)(d) illustrate the performance under the MiniImagenet 5-way, 5-shot scenario.

Table 18: Effect of skewed Beta distribution (i.e., $\lambda \sim \text{Beta}(\alpha, \beta)$ and $\alpha \neq \beta$) under the MiniImagenet 5-shot setting.

Settings	$\alpha = 0.5$	$\alpha = 1.0$	$\alpha = 2.0$	no MetaMix
$\beta = 0.5$	$55.35 \pm 0.96\%$	$53.82 \pm 0.99\%$	$53.05 \pm 0.93\%$	
$\beta = 1.0$	$53.38 \pm 0.94\%$	$56.12 \pm 1.02\%$	$54.91 \pm 1.01\%$	$51.95 \pm 0.97\%$
$\beta = 2.0$	$50.01 \pm 0.96\%$	$53.69 \pm 0.96\%$	$57.55 \pm 0.97\%$	

F.5 Boundary Analysis

In this section, we detail the way to visualize the decision boundary of MAML and MAML-MetaMix. Follow [19], we conduct a binary classification problem by using two columns of parameters in the final fully connected layer (i.e., \mathbf{w}_{f_1} , \mathbf{w}_{f_2} , b_{f_1} , b_{f_2}). In this work, we visualize the projections of hidden representations \mathbf{X}_{L-1} by the last layer. The X-coordinate \hat{x}_{proj} and Y-coordinate \hat{y}_{proj} are calculated as:

$$\hat{x}_{proj} = \mathbf{X}_{L-1} \frac{\mathbf{w}_{f_1} - \mathbf{w}_{f_2}}{\|\mathbf{w}_{f_1} - \mathbf{w}_{f_2}\|}, \quad \hat{y}_{proj} = \text{tSNE}(\mathbf{X}_{L-1} - \hat{x}_{proj} \frac{(\mathbf{w}_{f_1} - \mathbf{w}_{f_2})^\top}{\|\mathbf{w}_{f_1} - \mathbf{w}_{f_2}\|}), \quad (26)$$

where t-SNE [24] is applied for projecting the representation to 1-dimensional space. The decision boundary between two classes is further projected to a vertical line on the X-axis, which is formulated as:

$$\hat{x}_{d,proj} = -\frac{b_{f_1} - b_{f_2}}{\|\mathbf{w}_{f_1} - \mathbf{w}_{f_2}\|}. \quad (27)$$

Besides the case in the original paper, we illustrate more cases in Figure 12, which further support our conclusion that MetaMix encourages the representations to be more compact and improve the meta-generalization capability.

References

- [1] Martín Abadi, Paul Barham, Jianmin Chen, Zhifeng Chen, Andy Davis, Jeffrey Dean, Matthieu Devin, Sanjay Ghemawat, Geoffrey Irving, Michael Isard, et al. Tensorflow: a system for large-scale machine learning. In *OSDI*, volume 16, pages 265–283, 2016.
- [2] Alessandro Achille and Stefano Soatto. Information dropout: Learning optimal representations through noisy computation. *T-PAMI*, 40(12):2897–2905, 2018.
- [3] Alexander A Alemi, Ian Fischer, Joshua V Dillon, and Kevin Murphy. Deep variational information bottleneck. In *ICLR*, 2017.
- [4] Antreas Antoniou, Harrison Edwards, and Amos Storkey. How to train your maml. In *ICLR*, 2019.
- [5] Ekin D Cubuk, Barret Zoph, Dandelion Mane, Vijay Vasudevan, and Quoc V Le. Autoaugment: Learning augmentation strategies from data. In *CVPR*, pages 113–123, 2019.
- [6] Zi-Yi Dou, Keyi Yu, and Antonios Anastasopoulos. Investigating meta-learning algorithms for low-resource natural language understanding tasks. In *EMNLP*, 2019.
- [7] Chelsea Finn, Pieter Abbeel, and Sergey Levine. Model-agnostic meta-learning for fast adaptation of deep networks. In *ICML*, pages 1126–1135, 2017.
- [8] Chelsea Finn and Sergey Levine. Meta-learning and universality: Deep representations and gradient descent can approximate any learning algorithm. *arXiv preprint arXiv:1710.11622*, 2017.
- [9] Chelsea Finn, Kelvin Xu, and Sergey Levine. Probabilistic model-agnostic meta-learning. *NeurIPS*, 2018.
- [10] Sebastian Flennerhag, Andrei A Rusu, Razvan Pascanu, Hujun Yin, and Raia Hadsell. Meta-learning with warped gradient descent. In *ICLR*, 2020.
- [11] Yarin Gal and Zoubin Ghahramani. Dropout as a bayesian approximation: Representing model uncertainty in deep learning. In *ICML*, pages 1050–1059, 2016.
- [12] Erin Grant, Chelsea Finn, Sergey Levine, Trevor Darrell, and Thomas Griffiths. Recasting gradient-based meta-learning as hierarchical bayes. In *ICLR*, 2018.

- [13] Jiatao Gu, Yong Wang, Yun Chen, Kyunghyun Cho, and Victor OK Li. Meta-learning for low-resource neural machine translation. In *EMNLP*, 2018.
- [14] Geoffrey Hinton, Oriol Vinyals, and Jeff Dean. Distilling the knowledge in a neural network. *arXiv preprint arXiv:1503.02531*, 2015.
- [15] Muhammad Abdullah Jamal and Guo-Jun Qi. Task agnostic meta-learning for few-shot learning. In *CVPR*, pages 11719–11727, 2019.
- [16] Bingyi Kang, Zhuang Liu, Xin Wang, Fisher Yu, Jiashi Feng, and Trevor Darrell. Few-shot object detection via feature reweighting. In *ICCV*, pages 8420–8429, 2019.
- [17] Anders Krogh and John A Hertz. A simple weight decay can improve generalization. In *NeurIPS*, pages 950–957, 1992.
- [18] Brenden Lake, Ruslan Salakhutdinov, Jason Gross, and Joshua Tenenbaum. One shot learning of simple visual concepts. In *Proceedings of the annual meeting of the cognitive science society*, volume 33, 2011.
- [19] Hae Beom Lee, Taewook Nam, Eunho Yang, and Sung Ju Hwang. Meta dropout: Learning to perturb latent features for generalization. In *ICLR*, 2020.
- [20] Yoonho Lee and Seungjin Choi. Gradient-based meta-learning with learned layerwise metric and subspace. In *ICML*, pages 2933–2942, 2018.
- [21] Zhenguo Li, Fengwei Zhou, Fei Chen, and Hang Li. Meta-sgd: Learning to learn quickly for few shot learning. *arXiv preprint arXiv:1707.09835*, 2017.
- [22] Ming-Yu Liu, Xun Huang, Arun Mallya, Tero Karras, Timo Aila, Jaakko Lehtinen, and Jan Kautz. Few-shot unsupervised image-to-image translation. In *ICCV*, pages 10551–10560, 2019.
- [23] David Lopez-Paz, Léon Bottou, Bernhard Schölkopf, and Vladimir Vapnik. Unifying distillation and privileged information. *ICLR*, 2016.
- [24] Laurens van der Maaten and Geoffrey Hinton. Visualizing data using t-sne. *JMLR*, 9(Nov):2579–2605, 2008.
- [25] Andrea Madotto, Zhaojiang Lin, Chien-Sheng Wu, and Pascale Fung. Personalizing dialogue agents via meta-learning. In *ACL*, 2019.
- [26] Eric J Martin, Valery R Polyakov, Xiang-Wei Zhu, Li Tian, Prasenjit Mukherjee, and Xin Liu. All-assay-max2 pqsar: Activity predictions as accurate as four-concentration ic50s for 8558 novartis assays. *Journal of chemical information and modeling*, 59(10):4450–4459, 2019.
- [27] Nikhil Mishra, Mostafa Rohaninejad, Xi Chen, and Pieter Abbeel. A simple neural attentive meta-learner. *ICLR*, 2018.
- [28] Behnam Neyshabur, Srinadh Bhojanapalli, and Nathan Srebro. A PAC-bayesian approach to spectrally-normalized margin bounds for neural networks. In *ICLR*, 2018.
- [29] Alex Nichol, Joshua Achiam, and John Schulman. On first-order meta-learning algorithms. *arXiv preprint arXiv:1803.02999*, 2018.

- [30] Boris Oreshkin, Pau Rodríguez López, and Alexandre Lacoste. Tadam: Task dependent adaptive metric for improved few-shot learning. In *NeurIPS*, pages 721–731, 2018.
- [31] Eunbyung Park and Junier B Oliva. Meta-curvature. In *NeurIPS*, pages 3309–3319, 2019.
- [32] Aniruddh Raghu, Maithra Raghu, Samy Bengio, and Oriol Vinyals. Rapid learning or feature reuse? towards understanding the effectiveness of maml. In *ICLR*, 2020.
- [33] Sachin Ravi and Hugo Larochelle. Optimization as a model for few-shot learning. *ICLR*, 2016.
- [34] Ravid Shwartz-Ziv and Naftali Tishby. Opening the black box of deep neural networks via information. *arXiv preprint arXiv:1703.00810*, 2017.
- [35] Jake Snell, Kevin Swersky, and Richard Zemel. Prototypical networks for few-shot learning. In *NIPS*, pages 4077–4087, 2017.
- [36] Nitish Srivastava, Geoffrey Hinton, Alex Krizhevsky, Ilya Sutskever, and Ruslan Salakhutdinov. Dropout: a simple way to prevent neural networks from overfitting. *JMLR*, 15(1):1929–1958, 2014.
- [37] Flood Sung, Yongxin Yang, Li Zhang, Tao Xiang, Philip HS Torr, and Timothy M Hospedales. Learning to compare: Relation network for few-shot learning. In *CVPR*, pages 1199–1208, 2018.
- [38] Sebastian Thrun and Lorien Pratt. *Learning to learn*. Springer Science & Business Media, 1998.
- [39] Naftali Tishby and Noga Zaslavsky. Deep learning and the information bottleneck principle. In *2015 IEEE Information Theory Workshop (ITW)*, pages 1–5. IEEE, 2015.
- [40] Vikas Verma, Alex Lamb, Christopher Beckham, Amir Najafi, Ioannis Mitliagkas, Aaron Courville, David Lopez-Paz, and Yoshua Bengio. Manifold mixup: Better representations by interpolating hidden states. *ICML*, 2019.
- [41] Oriol Vinyals, Charles Blundell, Timothy Lillicrap, Daan Wierstra, et al. Matching networks for one shot learning. In *NIPS*, pages 3630–3638, 2016.
- [42] Risto Vuorio, Shao-Hua Sun, Hexiang Hu, and Joseph J Lim. Multimodal model-agnostic meta-learning via task-aware modulation. In *NeurIPS*, pages 1–12, 2019.
- [43] Yu Xiang, Roozbeh Mottaghi, and Silvio Savarese. Beyond pascal: A benchmark for 3d object detection in the wild. In *WACV*, pages 75–82. IEEE, 2014.
- [44] Annie Xie, Avi Singh, Sergey Levine, and Chelsea Finn. Few-shot goal inference for visuomotor learning and planning. In *CoRL*, pages 40–52, 2018.
- [45] Huaxiu Yao, Ying Wei, Junzhou Huang, and Zhenhui Li. Hierarchically structured meta-learning. In *ICML*, 2019.
- [46] Huaxiu Yao, Xian Wu, Zhiqiang Tao, Yaliang Li, Bolin Ding, Ruirui Li, and Zhenhui Li. Automated relational meta-learning. In *ICLR*, 2020.
- [47] Mingzhang Yin, George Tucker, Mingyuan Zhou, Sergey Levine, and Chelsea Finn. Meta-learning without memorization. *ICLR*, 2020.

- [48] Sung Whan Yoon, Jun Seo, and Jaekyun Moon. Tapnet: Neural network augmented with task-adaptive projection for few-shot learning. In *ICML*, 2019.
- [49] Tianhe Yu, Chelsea Finn, Annie Xie, Sudeep Dasari, Tianhao Zhang, Pieter Abbeel, and Sergey Levine. One-shot imitation from observing humans via domain-adaptive meta-learning. In *RSS*, 2018.
- [50] Hongyi Zhang, Moustapha Cisse, Yann N Dauphin, and David Lopez-Paz. mixup: Beyond empirical risk minimization. In *ICLR*, 2018.
- [51] Zhun Zhong, Liang Zheng, Guoliang Kang, Shaozi Li, and Yi Yang. Random erasing data augmentation. In *AAAI*, 2020.
- [52] Luisa M Zintgraf, Kyriacos Shiarlis, Vitaly Kurin, Katja Hofmann, and Shimon Whiteson. Fast context adaptation via meta-learning. In *ICML*, 2019.

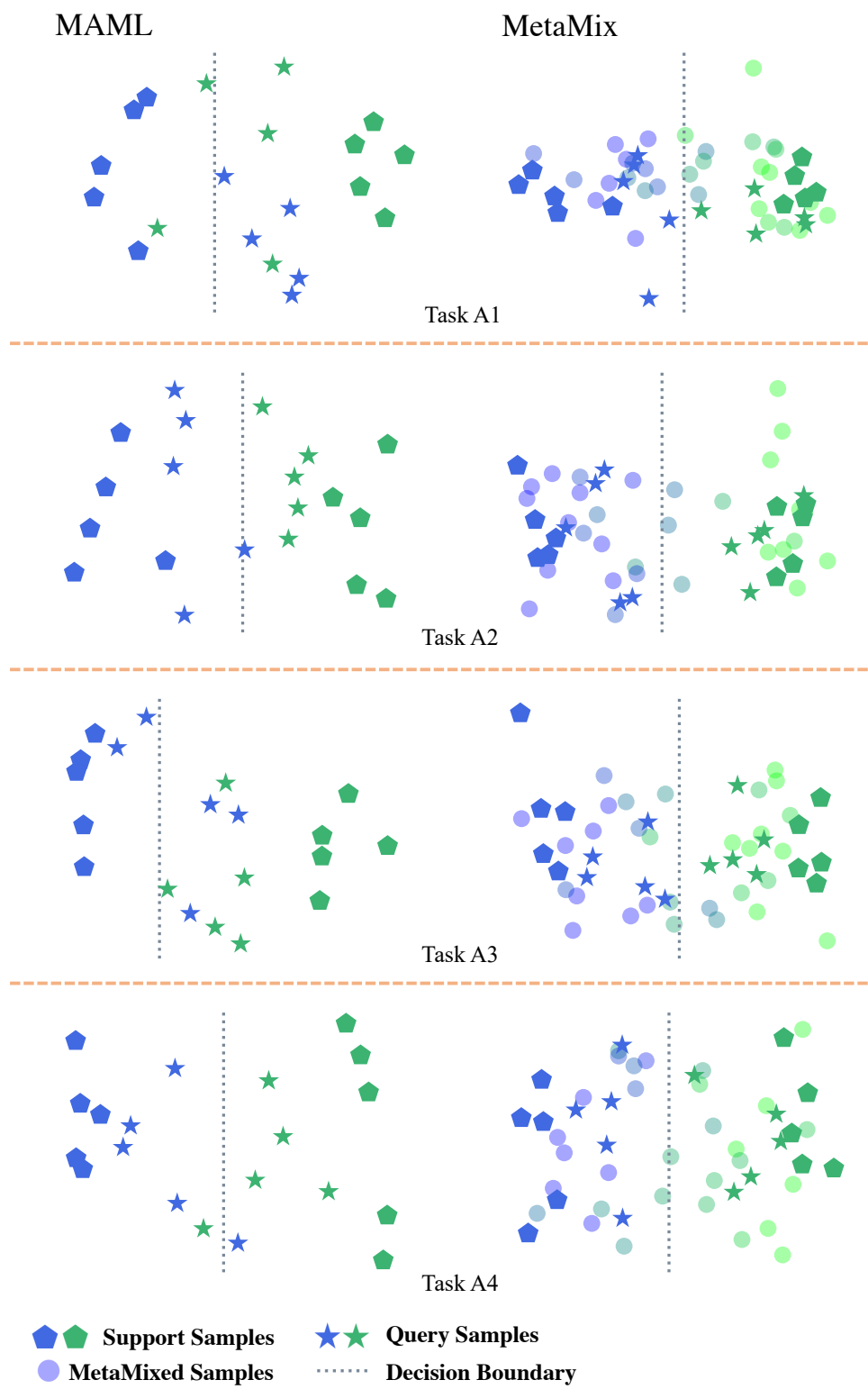


Figure 12: Visualization of decision boundaries for additional four tasks (i.e., Task A1-A4).